Reducing internal variables and improving efficiency in data-driven modelling of anisotropic damage from RVE simulations

Julien Yvonnet, Qi-Chang He, Pengfei Li

Reducing internal variables and improving efficiency in data-driven modelling of anisotropic damage from RVE simulations

Julien Yvonnet[1*], Qi-Chang He[1] and Pengfei Li[1]

[1]Univ Gustave Eiffel, MSME, CNRS UMR 8208, F-77454 Marne-la-Vallée, France.

*Corresponding author(s). E-mail(s): julien.yvonnet@univ-eiffel.fr;

Abstract

The Data-Driven Harmonic Analysis of Damage (DDHAD) has been proposed recently to construct arbitrarily anisotropic damage models in quasi-brittle heterogeneous materials from calculations on Representative Volume Elements (RVE). During preliminary off-line calculations, numerical crack propagations are simulated and the effective damaged elasticity tensor is computed by numerical homogenization. A macroscopic damage model with internal variables is defined using harmonic analysis of the elasticity tensor. The method, called Data-Driven Harmonic Analysis of Damage (DDHAD), is in this work improved by two key novelties. First, a numerical framework is proposed to evaluate efficiently the model during on-line calculations by computing all the integral terms during off-line calculations and expressing the damage model in a compact matrix form. Second, a reduced model is introduced to further reduce the number of internal variables which is in general large in 3D. It is shown in an application to the damage of 3D printed lattice that even for a complex 3D induced anisotropy, the number of internal variables can drop to a very small number (3 or 4) with the aid of the proposed strategy.

Keywords: Data-Driven method, Fracture, Damage, Multiscale, Homogenization

1 Introduction

Multiscale modeling of fracture in heterogeneous materials is a key problem in engineering for the design of more resistant materials, or for better understanding the mechanisms leading to higher strength from microstructural information. With the rapid growth of advanced manufacturing technologies such as e.g. 3D printing and additive manufacturing, it is today possible to create materials by design, i.e. designing the microstructure to obtain specific properties. However, predicting the strength of a material, given the sole knowledge of a Representative Volume Element (RVE), is highly challenging.

The most common approach in damage modeling is to define an empirical model for the equivalent homogeneous medium, and to identify the parameters of this model, either using experimental results, or using numerical microstructural simulations on the RVE. Another approach is the use of multiscale modeling, whose aim is to construct directly the behavior of the equivalent homogeneous medium from the RVE. In this work, only RVEs with quasi-brittle phases will be considered.

The numerical multiscale damage modeling problem can be formulated as follows: given an RVE, which can have an idealized or realistic microstructure, and given a numerical crack propagation method allowing to simulate the initiation and propagation of micro cracks within the RVE, how to define a damage model for the equivalent homogeneous medium? This problem induces several tough difficulties: (i) the lack of unified definition for the RVE in this situation; (ii) the numerical complexity of the micro crack propagation within an RVE; (iii) the definition of appropriate internal variables for the homogenized model, able to take into account initial and induced anisotropies; (iv) the definition of a model relating the effective elasticity tensor to the internal variables; (v) the definition of evolution laws for the internal variables; (vi) the definition of a practical procedure to relate the results of the RVE crack simulations to the homogenized model.

Point (i) has been discussed in numerical studies (see e.g. [1–3]), showing that RVEs for quasi-brittle fractured microstructures could be defined in particular situations. Issue (ii) can be alleviated using recent techniques like the phase field method [4–9]. This technique derives from a variational approach to fracture and leads to a simple and robust method to simulate the initiation, propagation, merging of multiple 2D and 3D cracks with arbitrary geometries while using simple numerical methods like the Finite Elements (see [8, 9] for a review of the phase field method and recent developments). The problem (iii) of defining the internal variables for an arbitrary anisotropic damage model is central and highly challenging [10]. Many damage variables models were proposed, including scalar [11, 12], second-order [13], fourth-order [14–22] or even eighth-order [23, 24] tensors.

Ladevèze [25], and He and Curnier [26, 27], have shown that arbitrarily anisotropic damage models can be described by damage surfaces associated with the orientated distribution functions. It was demonstrated in the mentioned papers that given these functions, the damaged elasticity tensor is completely and uniquely determined, providing a solution for problem (iv) in an elegant manner. To discretize these damage surfaces, the same authors proposed to describe it by Fourier series, and to use the coefficients of the Fourier series as internal variables. Regarding point (v), evolution laws in this context have been proposed in [13] with application to the damage of orthotropic materials. However, the mentioned works did not provide solutions to the issue (vi). Some recent works have provided alternative to point (iv), by using machine learning and data-driven approaches, for more general multiscale history-dependent [28–32] or damage problems [33–36] .

In the present work, we address points (iii), (iv) and (vi), while point (v) is reported to future studies. The present approach, named Data-Driven Harmonic Analysis Damage (DDHAD) method, uses the following ingredients: first, the above-mentioned Ladevèze-He-Curnier framework for defining a general anisotropic damage through orientation distribution functions is employed. Then, the phase field method is used to perform numerical crack simulations on RVE for different loading conditions, which serve as numerical data to construct the macroscopic model. Using these data, the damage orientation functions are identified by Fourier Series approximation. In our previous work [37], the coefficients of the Fourier series were taken as the discrete set of internal variables for the damage model. In this work, a Proper Orthogonal Decomposition (POD) reduced order model is employed to parametrize the orientation functions with a very small number of coefficients, which act as the new internal variables. As a result, a general anisotropic damage model can be defined and takes a remarkably simple form. A computational procedure is described to evaluate efficiently the damaged elasticity tensor. Detailed formulations and numerical implementations are provided for both 2D and 3D. The method is applied to the damage modeling of a 3D printed lattice RVE, to illustrate the accuracy of the method.

The outline of this article is as follows. In section 2, computational homogenization of cracked elastic material based on RVE is first reviewed. In section 3, the Data-Driven Harmonic Analysis-based Damage method (DDHAD), as introduced in our previous work [37], is presented. In section 4, a new computational framework for DDHAD is developed, to efficiently evaluate the damaged effective elastic tensor and provide the corresponding anisotropic damage model in a simple form, using pre-computed operators. In section

6, a further improvement is proposed by performing a reduction of the internal variables using POD. The overall procedure is summarized in section 7. Finally, the technique is illustrated on the damage of an anisotropic 3D lattice RVE in section 8.

2 Computational homogenization of cracked elastic solids

We now briefly review the basics of linear computational homogenization with a Representative Volume Element (RVE). More details can be found e.g. in [38–40]. We consider an RVE defined in a domain $\Omega \subset \mathbb{R}^{dim}$, with dim denoting the space dimension. Let $\overline{\boldsymbol{\varepsilon}}$ be the macroscopic strain tensor and $\boldsymbol{\varepsilon}$ its microscopic counterpart. Under the assumption of scale separation, the former is defined as the volume average of the latter

$$\overline{\boldsymbol{\varepsilon}} = \frac{1}{|\Omega|}\int_{\Omega} \boldsymbol{\varepsilon} d\Omega, \tag{1}$$

which holds only if the RVE does not contain any sharp cracks, imperfectly bounded interfaces or voids and where $\boldsymbol{\varepsilon} = \frac{1}{2}\left(\nabla \mathbf{u} + \nabla^T \mathbf{u}\right)$. In the case where $\mathbf{u}$ is not continuously differentiable, the previous definition must be replaced by

$$\overline{\boldsymbol{\varepsilon}} = \frac{1}{2|\Omega|}\int_{\Omega} \left(\mathbf{u} \otimes \mathbf{x} + \mathbf{x} \otimes \mathbf{u}\right) d\Gamma, \tag{2}$$

where $\mathbf{x}$ is the position vector of a point within the RVE. Similarly, the macro stress tensor $\overline{\boldsymbol{\sigma}}$ in terms of its microscopic counterpart $\boldsymbol{\sigma}$ is given by:

$$\overline{\boldsymbol{\sigma}} = \frac{1}{|\Omega|}\int_{\Omega} \boldsymbol{\sigma} d\Omega, \tag{3}$$

which holds if the domain does not contain sharp cracks or imperfectly bounded interfaces. In the following, a regularized description of discontinuities will be adopted to describe the cracks and thus the above assumption will hold. Assuming quasi-static load and elastic damage at each incremental load, the effective elastic tensor $\overline{\mathbb{C}}(t)$ at each load step (denoted here as time t) can be computed as follows. First, at one load step t, the following boundary conditions on the surface $\partial\Omega$ of the RVE can be prescribed:

$$\mathbf{u}(\mathbf{x}) = \overline{\boldsymbol{\varepsilon}}\mathbf{x} + \tilde{\mathbf{u}}(\mathbf{x}) \ \text{ on } \partial\Omega, \tag{4}$$

where $\tilde{\mathbf{u}}$ represents a periodic fluctuation over Ω. Solving the linear problem

$$\nabla \cdot \boldsymbol{\sigma} = 0 \ \text{ in } \Omega, \tag{5}$$

where $\nabla \cdot (.)$ denotes the divergence operator and $\boldsymbol{\sigma}(\mathbf{x}) = \mathbb{C}(\mathbf{x}, t) : \boldsymbol{\varepsilon}(\mathbf{x})$, the localization tensor at load t can be written as

$$A_{ijkl}(\mathbf{x}, t) = \varepsilon_{ij}^{(kl)}(\mathbf{x}, t) \tag{6}$$

where $\varepsilon_{ij}^{(kl)}$ is the strain solution of the above problem when $\overline{\boldsymbol{\varepsilon}} = \frac{1}{2}\left(\mathbf{e}_k \otimes \mathbf{e}_l + \mathbf{e}_l \otimes \mathbf{e}_k\right)$. Then, at each time t the following linear relationship can be established, using the superposition principle, as:

$$\boldsymbol{\varepsilon}(\mathbf{x}, t) = \mathbb{A}(\mathbf{x}, t) : \overline{\boldsymbol{\varepsilon}}(t) \tag{7}$$

and

$$\boldsymbol{\sigma}(\mathbf{x}, t) = \mathbb{C}(\mathbf{x}, t) : \mathbb{A}(\mathbf{x}, t) : \overline{\boldsymbol{\varepsilon}}. \tag{8}$$

Finally, averaging over Ω, we obtain the macro stress-strain relationship:

$$\overline{\boldsymbol{\sigma}}(t) = \overline{\mathbb{C}}(t) : \overline{\boldsymbol{\varepsilon}}(t) \tag{9}$$

with

$$\overline{\mathbb{C}}(t) = \frac{1}{|\Omega|}\int_{\Omega} \mathbb{C}(\mathbf{x}, t) : \mathbb{A}(\mathbf{x}, t) d\Omega, \tag{10}$$

still assuming the absence of sharp cracks or cohesive interfaces within the RVE (see [40] for extended definitions of the macro stress when the mentioned assumption does not hold).

3 Harmonic analysis applied to anisotropic damage modeling

3.1 Harmonic description of the elasticity tensor

The Data-Driven Harmonic Analysis-based Damage (DDHAD) modeling has been introduced in our previous work [37] and is here developed for efficient computational implementation. The starting point of harmonic analysis-based damage models [25, 26, 41] is the use of scalar orientation distribution functions (ODFs) to describe an

isotropic or arbitrary anisotropic elasticity tensor. These functions can be developed into two Fourier series. Truncating these series, a reduced parameterization of the elasticity tensor can be obtained. Ladevèze [25, 41], and He and Curnier [26] used this idea to define damage models through damage ODFs, from which the associated damaged anisotropic elasticity tensor can be reconstructed. In this section, the basics of elasticity tensor reconstruction from ODFs is briefly reviewed. It can be shown (see e.g. [26]) that two ODFs are sufficient to completely describe a fourth-order elasticity tensor. These two functions are defined by:

$$\eta(\mathbf{n}) = n_i n_j n_k n_l \overline{C}_{ijkl}, \tag{11}$$

$$\kappa(\mathbf{n}) = \delta_{ij} n_k n_l \overline{C}_{ijkl}, \tag{12}$$

where $\mathbf{n}$ is a unitary orientation vector (see Fig. 1) and $\overline{\mathbb{C}}$ is the effective elasticity tensor associated with the RVE. Given the microstructure of the RVE and its local elastic properties, $\overline{\mathbb{C}}$ can be computed numerically using computational homogenization. For the sake of conciseness, the interested reader can refer to e.g. [40] for a detailed presentation and practical implementation of computational homogenization. The orientation functions $\eta(\mathbf{n})$ and $\kappa(\mathbf{n})$ define the elongation and bulk moduli along the direction $\mathbf{n}$, respectively.

The elasticity tensor $\overline{\mathbb{C}}$ can be fully recovered from $\eta(\mathbf{n})$ and $\kappa(\mathbf{n})$ as follows. In 2D, the orientation functions can be parameterized by an angle $\theta \in [-\pi;\ \pi]$ (see Fig. 1 (a)), then $\eta(\mathbf{n}) \equiv \eta(\theta)$ and $\kappa(\mathbf{n}) \equiv \kappa(\theta)$. The irreducible form of the elasticity tensor is in the 2D case given by [42, 43]:

$$\overline{\mathbb{C}} = \lambda \mathbf{I} \otimes \mathbf{I} + \mu \mathbf{I} \underline{\otimes} \mathbf{I} + \mathbf{I} \otimes \mathbf{A} + \mathbf{A} \otimes \mathbf{I}$$

$$+ \mathbf{I} \underline{\otimes} \mathbf{A} + \mathbf{A} \underline{\otimes} \mathbf{I} + \mathbb{Z} \tag{13}$$

where λ and μ are the Lamé's coefficients, $\mathbf{I}$ is the second-order identity tensor, $\mathbf{A}$ is a traceless symmetric second-order tensor and $\mathbb{Z}$ is a fourth-order completely symmetric traceless tensor. Above, $(\mathbf{A} \underline{\otimes} \mathbf{B})_{ijkl} = (A_{ik}B_{jl} + A_{il}B_{jk})$. Theses different quantities are related to the ODFs $\eta(\theta)$ and $\kappa(\theta)$ as follows [27]:

$$\lambda = v - u, \quad \mu = u - \frac{v}{2}, \quad \mathbf{A} = \frac{1}{6}\mathbf{V}, \tag{14}$$

$$u = \frac{1}{2\pi}\int_{-\pi}^{\pi} \eta(\theta) d\theta, \quad v = \frac{1}{2\pi}\int_{-\pi}^{\pi} \kappa(\theta) d\theta, \tag{15}$$

$$\mathbf{V} = \frac{2}{\pi}\int_{-\pi}^{\pi} \eta(\theta)\mathbf{F}(\theta) d\theta, \quad \mathbb{Z} = \frac{8}{\pi}\int_{-\pi}^{\pi} \eta(\theta)\mathbb{F}(\theta) d\theta, \tag{16}$$

where $\mathbf{F}(\theta)$ and $\mathbb{F}(\theta)$ denote generalized spherical harmonics. The expressions of $\mathbf{F}$ and $\mathbb{F}$ are provided in Appendix A. The irreducible form of the 3D elasticity tensor and its reconstruction from 3D ODFs are provided in Appendix B.

3.2 Harmonic analysis-based damage model

Based on the results recalled above, a general damage model can be constructed by defining two damage ODFs $d(\mathbf{n})$ and $h(\mathbf{n})$ according to:

$$\begin{cases} \eta(\mathbf{n}, t) = [1 - d(\mathbf{n}, t)]\, \eta_0(\mathbf{n}) \\ \kappa(\mathbf{n}, t) = [1 - h(\mathbf{n}, t)]\, \kappa_0(\mathbf{n}) \end{cases} \tag{17}$$

where $\eta(\mathbf{n}, t)$ and $\kappa(\mathbf{n}, t)$ change with respect to a pseudo time t (here associated with a quasi-static load) evolution), and are defined by

$$\eta(\mathbf{n}, t) = n_i n_j n_k n_l \overline{C}_{ijkl}(t), \tag{18}$$

$$\kappa(\mathbf{n}, t) = \delta_{ij} n_k n_l \overline{C}_{ijkl}(t), \tag{19}$$

where $\overline{\mathbb{C}}(t)$ is the damaged elasticity tensor. This damaged elasticity tensor can be evaluated by computational homogenization on a Representative Volume Element (RVE) of a microstructure subjected to a loading evolving with as a function of t. The local evolution of damage within the RVE can be computed numerically using crack propagation simulation methods (XFEM [44], nonlocal damage models [45], cohesive elements [46], or phase field [4–8], among many others techniques). In the present work, the phase field method is employed. To avoid overburdening the paper, we report the description of the phase field method e.g. to the review papers [8, 9]. Then, given a cracked microstructure at time t, and using computational homogenization [37], the effective elasticity tensor $\overline{\mathbb{C}}(t)$ can be computed and stored for each time step t (or quasi-static load). The functions $\eta_0(\mathbf{n}) \equiv \eta(\mathbf{n}, t = 0)$ and $\kappa_0(\mathbf{n}) \equiv \kappa(\mathbf{n}, t = 0)$ denote the moduli of the undamaged RVE.

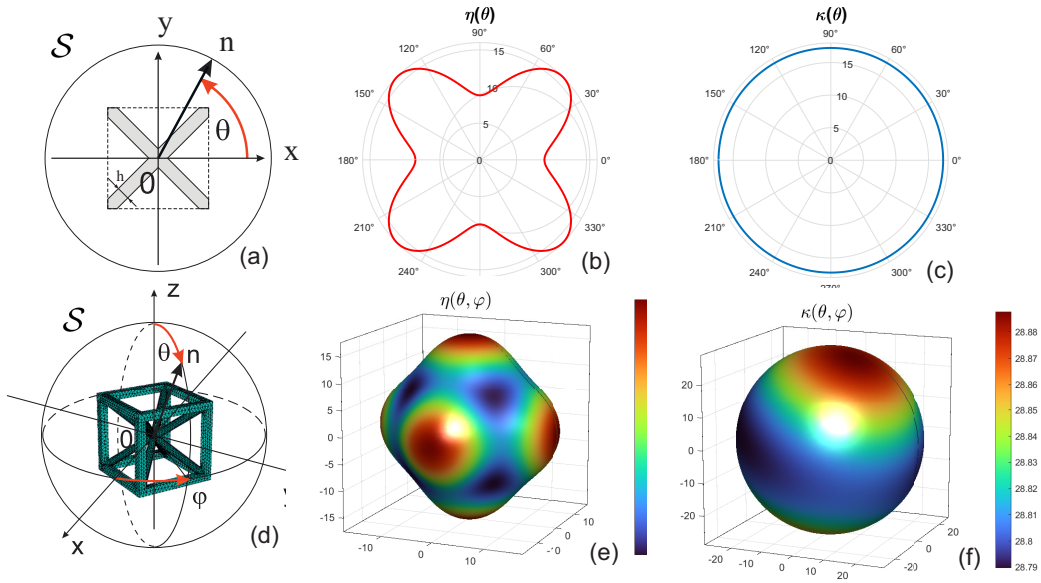

Fig. 1 (a) 2D Representative volume element (RVE) and orientation vector $\mathbf{n}$ in polar coordinates; (b) 2D elongation orientation function $\eta(\mathbf{n})$ (c) 2D bulk modulus orientation function $\kappa(\mathbf{n})$; (d) 3D RVE and orientation vector $\mathbf{n}$ in spherical coordinates; (e) 3D elongation orientation function $\eta(\mathbf{n})$; (f) 3D bulk modulus orientation function $\kappa(\mathbf{n})$.

Then, given $d(\mathbf{n},t)$ and $h(\mathbf{n},t)$ at any time t, the elasticity tensor can be fully reconstructed from (17) and (13)-(16) in 2D or (B12)-(B19) in 3D. In a non-classical manner, $d(\mathbf{n},t)$ and $h(\mathbf{n},t)$ constitute internal variables, but in the form of continuous surfaces. Obviously, a finite number of scalar variables is preferable. The key idea is to parametrize these functions by using Fourier series (see [47–49]):

$$f(\mathbf{n}) = g + \mathbf{G} : \mathbf{F}(\mathbf{n}) + \mathbb{G} :: \mathbb{F}(\mathbf{n}) + \ldots \quad , \tag{20}$$

where g, $\mathbf{G}$, $\mathbb{G}$ denote zero-order, second-order and fourth-order spherical harmonics, respectively, and are specified below for the 2D case and in Appendix C for the 3D case. In (20), $\mathbb{A} :: \mathbb{B} = A_{ijkl}B_{ijkl}$.

Expressing $d(\mathbf{n})$ and $h(\mathbf{n})$ in the form (20), the coefficients of the Fourier series can be used as a finite number of scalar internal variables. This number seems large at first glance. However, using the properties of $\overline{\mathbb{C}}$, $\mathbf{F}$ and $\mathbb{F}$, it has been shown in [26] and specified in [37] that the total number of independent Fourier coefficients required to reconstruct the elasticity tensor can be reduced to 6 in 2D and 21 in 3D. In practice, the Fourier series can be truncated to further reduce this number [37].

In 2D, using (20), the expansions of d and h reduce to [27]:

$$d(\theta,t) = d_0(t) + \mathbf{D}(t) : \mathbf{F}(\theta) + \mathbb{D}(t) :: \mathbb{F}(\theta), \tag{21}$$

$$h(\theta,t) = h_0(t) + \mathbf{D}(t) : \mathbf{F}(\theta), \tag{22}$$

with

$$d_0(t) = \frac{1}{2\pi}\int_{-\pi}^{\pi} d(\theta,t)d\theta, \tag{23}$$

$$h_0(t) = \frac{1}{2\pi}\int_{-\pi}^{\pi} h(\theta,t)d\theta, \tag{24}$$

and

$$\mathbf{D} = \frac{2}{\pi}\int_{-\pi}^{\pi} d(\theta,t)\mathbf{F}(\theta)d\theta, \tag{25}$$

$$\mathbb{D} = \frac{8}{\pi}\int_{-\pi}^{\pi} d(\theta,t)\mathbb{F}(\theta)d\theta. \tag{26}$$

These coefficients are computed numerically and stored as data for each time step. Then, for a given time t, $\eta(\theta,t)$ and $\kappa(\theta,t)$ can be reconstructed according to (21)-(22) and the elasticity tensor can be reconstructed by (17) and (13)-(16).

At this stage, all coefficients $d_0(t)$, $h_0(t)$, $\mathbf{D}(t)$ and $\mathbb{D}(t)$ constitute the set of internal variables.

However, the total number of independent internal variables may be reduced to 6 in 2D due to the symmetry properties of the tensors, as shown in the following. As $\mathbf{D}$ is traceless, then,

$$D_{22} = -D_{11}. \tag{27}$$

As $\mathbb{D}$ is Completely Symmetric and Traceless (CST) [26] (see (A4)), then,

$$D_{1122} = -D_{1111}, \quad D_{2222} = D_{1111}, \tag{28}$$

$$D_{2212} = -D_{1112}, \quad D_{1212} = -D_{1111}. \tag{29}$$

Then, a maximum number of 6 independent internal variables is sufficient to describe a general anisotropic 2D damage behavior, which are ordered as follows:

$$\boldsymbol{\alpha} = \{\alpha_1, \alpha_2, \alpha_3, \alpha_4, \alpha_5, \alpha_6\} \tag{30}$$

with

$$\alpha_1 = d_0, \quad \alpha_2 = h_0, \quad \alpha_3 = D_{11}, \quad \alpha_4 = D_{12},$$

$$\alpha_5 = D_{1111}, \quad \alpha_6 = D_{1112}. \tag{31}$$

The corresponding 3D formulation is provided in Appendix C.

4 Fast evaluation of internal variables in harmonic analysis-based damage model

It is worth noting that given the internal variables $\boldsymbol{\alpha}$, reconstructing the damaged elasticity tensor $\overline{\mathbb{C}}$ from (21)-(26), (17) and then (14) - (16), (13) involves many operations, including costly integral calculations. During on-line computations, it is desired to evaluate efficiently the elasticity tensor, given $\boldsymbol{\alpha}$. To address this issue, a fast procedure is proposed in the present paper, where all linear operators are associated with the above-mentioned steps pre-computed. As a result, a linear relationship between $\overline{\mathbb{C}}$ and the internal variables $\boldsymbol{\alpha}$ is provided. The procedure is first detailed here in the 2D case, using the linear damage model (17).

Using the notations defined in (31), the expansions (21)-(22) can be re-written as:

$$d(\theta) = \alpha_1 + \alpha_3 \left(F_{11}(\theta) - F_{22}(\theta)\right) + 2\alpha_4 F_{12}(\theta)$$

$$+\alpha_5 \left(F_{1111}(\theta) - 2F_{1122}(\theta) + F_{2222}(\theta) + F_{1212}(\theta)\right)$$

$$+\alpha_6 \left(2F_{1112}(\theta) - 2F_{2212}(\theta)\right), \tag{32}$$

$$h(\theta) = \alpha_2 + \alpha_3 \left(F_{11}(\theta) - F_{22}(\theta)\right) + 2\alpha_4 F_{12}(\theta). \tag{33}$$

Then, the following compact forms can be adopted:

$$d(\theta) = \mathbf{V}^d(\theta) \cdot \boldsymbol{\alpha}, \quad h(\theta) = \mathbf{V}^h(\theta) \cdot \boldsymbol{\alpha} \tag{34}$$

with $\boldsymbol{\alpha}^T = [\alpha_1, \alpha_2, , ..., \alpha_6]$ and

$$\mathbf{V}^d(\theta) =$$

$$= \begin{bmatrix} 1 \\ 0 \\ F_{11}(\theta) - F_{22}(\theta) \\ 2F_{12}(\theta) \\ F_{1111}(\theta) - 2F_{1122}(\theta) + F_{2222}(\theta) - 4F_{1212}(\theta) \\ 4F_{1112}(\theta) - 4F_{2212}(\theta) \end{bmatrix}, \tag{35}$$

$$\mathbf{V}^h(\theta) = \begin{bmatrix} 0 \\ 1 \\ F_{11}(\theta) - F_{22}(\theta) \\ 2F_{12}(\theta) \\ 0 \\ 0 \end{bmatrix}. \tag{36}$$

Expressing the ODFs together with the linear model (17), it yields:

$$u = u^0 - \mathbf{u}^d \cdot \boldsymbol{\alpha}, \quad v = v^0 - \mathbf{v}^h \cdot \boldsymbol{\alpha}, \tag{37}$$

$$V_{11} = V_{11}^0 - \mathbf{V}_{11}^d \cdot \boldsymbol{\alpha}, \quad V_{12} = V_{12}^0 - \mathbf{V}_{12}^d \cdot \boldsymbol{\alpha}, \tag{38}$$

$$Z_{1111} = Z^0_{1111} - \mathbf{Z}^d_{1111}\cdot\boldsymbol{\alpha},\;\; Z_{1112} = Z^0_{1112} - \mathbf{Z}^d_{1112}\cdot\boldsymbol{\alpha}, \tag{39}$$

with

$$\begin{aligned} u^0 &= \frac{1}{2\pi}\int_{-\pi}^{\pi}\eta_0(\theta)d\theta, \\ \mathbf{u}^d &= \frac{1}{2\pi}\left(\int_{-\pi}^{\pi}\eta_0(\theta)\mathbf{V}^d(\theta)d\theta\right), \end{aligned} \tag{40}$$

$$\begin{aligned} v^0 &= \frac{1}{2\pi}\int_{-\pi}^{\pi}\kappa_0(\theta)d\theta, \\ \mathbf{v}^h &= \frac{1}{2\pi}\left(\int_{-\pi}^{\pi}\kappa_0(\theta)\mathbf{V}^h(\theta)d\theta\right), \end{aligned} \tag{41}$$

$$V^0_{11} = \frac{2}{\pi}\int_{-\pi}^{\pi}\eta_0(\theta)F_{11}(\theta)d\theta,$$

$$\mathbf{V}^d_{11} = \left(\frac{2}{\pi}\int_{-\pi}^{\pi}\eta_0(\theta)F_{11}(\theta)\mathbf{V}^d(\theta)d\theta\right),$$

$$V^0_{12} = \frac{2}{\pi}\int_{-\pi}^{\pi}\eta_0(\theta)F_{12}(\theta)d\theta,$$

$$\mathbf{V}^d_{12} = \left(\frac{2}{\pi}\int_{-\pi}^{\pi}\eta_0(\theta)F_{12}(\theta)\mathbf{V}^d(\theta)d\theta\right),$$

$$Z^0_{1111} = \frac{8}{\pi}\int_{-\pi}^{\pi}\eta_0(\theta)F_{1111}(\theta)d\theta,$$

$$\mathbf{Z}^d_{1111} = \left(\frac{8}{\pi}\int_{-\pi}^{\pi}\eta_0(\theta)F_{1111}(\theta)\mathbf{V}^d(\theta)d\theta\right),$$

$$Z^0_{1112} = \frac{8}{\pi}\int_{-\pi}^{\pi}\eta_0(\theta)F_{1112}(\theta)d\theta,$$

$$\mathbf{Z}^d_{1112} = \left(\frac{8}{\pi}\int_{-\pi}^{\pi}\eta_0(\theta)F_{1112}(\theta)\mathbf{V}^d(\theta)d\theta\right).$$

All scalar quantities u^0, v^0, V^0_{11}, V^0_{12}, Z^0_{1111} and Z^0_{1112} as well as the vector quantities $\mathbf{u}^d$, $\mathbf{v}^d$, $\mathbf{V}^d_{11}$, $\mathbf{V}^d_{12}$, $\mathbf{Z}^d_{1111}$ and $\mathbf{Z}^d_{1112}$ can be pre-computed independently of $\boldsymbol{\alpha}$.

Using (13)-(16), the components of $\overline{\mathbb{C}}$ can be expressed as follows:

$$\overline{C}_{1111} = u + V_{11} + Z_{1111}$$

$$= \left(u^0 + V^0_{11} + Z^0_{1111}\right) - \left(\mathbf{u}^d + \mathbf{V}^d_{11} + \mathbf{Z}^d_{1111}\right)\cdot\boldsymbol{\alpha}, \tag{42}$$

$$\overline{C}_{1122} = v - u - Z_{1111}$$

$$= \left(v^0 - u^0 - Z^0_{1111}\right) - \left(\mathbf{v}^h - \mathbf{u}^d - \mathbf{Z}^d_{1111}\right)\cdot\boldsymbol{\alpha}, \tag{43}$$

$$\overline{C}_{1112} = \frac{1}{2}V_{12} + Z_{1112}$$

$$= \left(\frac{1}{2}V^0_{12} + Z^0_{1112}\right) - \left(\frac{1}{2}\mathbf{V}^d_{12} + \mathbf{Z}^d_{1112}\right)\cdot\boldsymbol{\alpha}, \tag{44}$$

$$\overline{C}_{2222} = u - V_{11} + Z_{1111}$$

$$= \left(u^0 - V^0_{11} + Z^0_{1111}\right) - \left(\mathbf{u}^d - \mathbf{V}^d_{11} + \mathbf{Z}^d_{1111}\right)\cdot\boldsymbol{\alpha}, \tag{45}$$

$$\overline{C}_{2212} = \frac{1}{2}V_{12} - Z_{1112}$$

$$= \left(\frac{1}{2}V^0_{12} - Z^0_{1112}\right) - \left(\frac{1}{2}\mathbf{V}^d_{12} - \mathbf{Z}^d_{1112}\right)\cdot\boldsymbol{\alpha}, \tag{46}$$

$$\overline{C}_{1212} = u - \frac{1}{2}v - Z_{1111}$$

$$= \left(u^0 - \frac{v^0}{2} - Z^0_{1111}\right) - \left(\mathbf{u}^d - \frac{\mathbf{v}^h}{2} - \mathbf{Z}^d_{1111}\right)\cdot\boldsymbol{\alpha}. \tag{47}$$

It is worth noting that the first terms of each components are the initial (undamaged) components of the effective elastic tensor. Then, these terms do not need to be computed as already known. The above form can be re-written as in a matrix form as:

$$[\overline{\mathbf{C}}(\boldsymbol{\alpha})] = [\overline{\mathbf{C}}^0] - \tilde{\mathbf{C}}\cdot\boldsymbol{\alpha}. \tag{48}$$

In (48) $[\overline{\mathbf{C}}(\boldsymbol{\alpha})]$ is a column vector containing the components of $\overline{\mathbb{C}}(\boldsymbol{\alpha})$ as

$$[\overline{\mathbf{C}}(\boldsymbol{\alpha})]^T = \left[\, C_{1111}(\boldsymbol{\alpha});\;\; C_{1122}(\boldsymbol{\alpha});\;\; C_{1112}(\boldsymbol{\alpha});\right.$$

$$C_{2222}(\boldsymbol{\alpha});\ C_{2212}(\boldsymbol{\alpha});\ C_{1212}(\boldsymbol{\alpha})\,\big] \tag{49}$$

and $\tilde{\mathbf{C}}$ is a matrix such that:

$$\tilde{\mathbf{C}} = \big[\,\mathbf{C}^T_{1111},\,\mathbf{C}^T_{1122},\,\mathbf{C}^T_{1112},\,\mathbf{C}^T_{2222},\,\mathbf{C}^T_{2212},\,\mathbf{C}^T_{1212}\,\big], \tag{50}$$

where $\mathbf{C}^T_{ijkl}$ are column vectors, whose specific expressions are given by

$$\mathbf{C}_{1111} = \mathbf{u}^d + \mathbf{V}^d_{11} + \mathbf{Z}^d_{1111},\ \ \mathbf{C}_{1122} = \mathbf{v}^h - \mathbf{u}^d - \mathbf{Z}^d_{1111}, \tag{51}$$

$$\mathbf{C}_{1112} = \frac{1}{2}\mathbf{V}^d_{12} + \mathbf{Z}^d_{1112},\ \ \mathbf{C}_{2222} = \mathbf{u}^d - \mathbf{V}^d_{11} + \mathbf{Z}^d_{1111}, \tag{52}$$

$$\mathbf{C}_{2212} = \frac{1}{2}\mathbf{V}^d_{12} - \mathbf{Z}^d_{1112},\ \ \mathbf{C}_{1212} = \mathbf{u}^d - \frac{\mathbf{v}^h}{2} - \mathbf{Z}^d_{1111}. \tag{53}$$

It is then only required to pre-compute the vector quantities $\mathbf{u}^d$, $\mathbf{v}^h$, $\mathbf{V}^d_{11}$, $\mathbf{V}^d_{12}$, $\mathbf{Z}^d_{1111}$ and $\mathbf{Z}^d_{1112}$.

Note that (48) can be re-written in tensor form as:

$$\overline{\mathbb{C}}\,(\boldsymbol{\alpha}(t)) = \overline{\mathbb{C}}^0 - \sum_{k=1}^{N} \overline{\mathbb{C}}^k \alpha_k(t) \tag{54}$$

where $\overline{\mathbb{C}}^0$ is the undamaged elastic tensor and

$$\overline{\mathbb{C}}^k = \int_{\mathcal{S}} \left[\mathbb{K}^\eta(\mathbf{n})\eta_0(\mathbf{n}) + \mathbb{K}^\kappa(\mathbf{n})\kappa_0(\mathbf{n})\right] d\mathcal{S}, \tag{55}$$

where $\mathbb{K}^\eta(\mathbf{n})$ and $\mathbb{K}^\kappa(\mathbf{n})$ are tensors independent of the RVE geometry, and $\mathcal{S}$ is the unit circle in 2D and the unit sphere in 3D (see Fig. 1). Furthermore, we also notice that the tensors $\overline{\mathbb{C}}^k$ only depend on the undamaged state of the RVE. In (54), N is the number of terms in the Fourier series. When the series is not truncated, the maximum value is $N = 6$ in 2D and $N = 21$ in 3D.

The full details to extend the above procedure to a 3D elastic tensor for the linear model is provided in Appendix D.

5 Summary of the previous version of the DDHAD method [37]

5.1 Off-line calculations: data generation

- Compute $[\mathbf{C}^0]$.
- Apply P loads on the RVE for n^p load increments
  At each load increment t^p_n:
  - Prescribe boundary conditions on the RVE and solve the crack propagation problem, e.g. using phase field method to fracture.
  - Compute and store $\overline{\mathbb{C}}(t^p_n)$ by computational homogenization for $n = 1, 2, ..., n^p$, $p = 1, 2, ..., P$.
- For all pre-computed values of $\overline{\mathbb{C}}(t^p_n)$, compute the internal variables $\boldsymbol{\alpha}$ as described in section 3.2.
- Select the relevant internal variables $\tilde{\boldsymbol{\alpha}}$ from $\boldsymbol{\alpha}$ by applying an appropriate criterion (see more details in [37]).

5.2 On-line calculations

At each load increment t^p_n, $p = 1, 2, ..., P^m$:

- Update internal variables $\tilde{\boldsymbol{\alpha}}(t^p_n)$ from the macro mechanical fields at t^{p-1}_n (note that this point remains to be developed, and is reported to future studies).
- Given $\tilde{\boldsymbol{\alpha}}(t^p_n)$, evaluate $\overline{\mathbb{C}}(t^p_n)$ by integral computations (55) and by (54).
- Solve the mechanical problem $\nabla\cdot\big(\overline{\mathbb{C}}(t^p_n) : \overline{\boldsymbol{\varepsilon}}\big) + \overline{\mathbf{b}} = 0$ in $\overline{\Omega}$.

Above, $\overline{\Omega}$ denotes the macroscopic domain, and $\overline{\mathbf{b}}$ is a body force therm at the macro scale.

6 Damage model with reduced internal variables

6.1 POD reduction of internal variables

In some situations where a strong anisotropy is present, truncating the Fourier series in (21)-(22) might still lead to a large number of internal variables. To further reduce this number, we propose here to use the Proper Orthogonal Decomposition

(POD) (see e.g. [50–53]) to capture the dominant elements in the internal variables evolution and remove high-order terms by expressing them through a reduced basis.

We define a matrix $\mathbf{Q}$ in which each column corresponds to the vector $\boldsymbol{\alpha}(t)$ at a load increment t, and which is obtained by the procedure described in section 3.2 during off-line calculations. Note that the realizations of $\boldsymbol{\alpha}(t)$ along several loading paths can be grouped in the matrix $\mathbf{Q}$. The dimensions of $\mathbf{Q}$ is then $(6 \times R)$ in 2D and $(21 \times R)$ in 3D, where R is the total number of load increments during the overall set of off-line calculations.

Then, the following eigenvalue problem is solved:

$$\left(\mathbf{Q}\mathbf{Q}^T\right)\boldsymbol{\phi}_k = \lambda_k \boldsymbol{\phi}_k \tag{56}$$

where $\boldsymbol{\phi}_k$ denotes the eigenvectors and λ_k denote the corresponding eigenvalues. The M eigenvectors associated with the M highest eigenvalues can be selected according to the criterion:

$$\frac{\lambda_i}{max\left(\lambda_i\right)} < \delta \tag{57}$$

where δ is a tolerance parameter. We define a matrix $\boldsymbol{\Phi}$ whose columns contain the corresponding M eigenvectors. Its size is $(6 \times M)$ in 2D and $(21 \times M)$ in 3D. Then, an approximation of $\boldsymbol{\alpha}(t)$ can be obtained as:

$$\boldsymbol{\alpha}(t) = \boldsymbol{\Phi}\boldsymbol{\beta}(t) \tag{58}$$

where $\boldsymbol{\beta}(t)$ is a $(M \times 1)$ vector of reduced internal variables. Given $\boldsymbol{\alpha}(t)$, the vector $\boldsymbol{\beta}(t)$ can be recovered at each time t by minimizing the distance between $\boldsymbol{\alpha}(t)$ and its approximation in the least square sense, i.e.:

$$\boldsymbol{\beta}(t) = Argmin(J),$$

$$J = \left(\boldsymbol{\alpha}(t) - \boldsymbol{\Phi}\boldsymbol{\beta}(t)\right) \cdot \left(\boldsymbol{\alpha}(t) - \boldsymbol{\Phi}\boldsymbol{\beta}(t)\right) \tag{59}$$

or

$$\frac{\partial J}{\partial \boldsymbol{\beta}(t)} = 0 \tag{60}$$

which leads to the following system that must be solved to obtain $\boldsymbol{\beta}(t)$:

$$\boldsymbol{\phi}^T\boldsymbol{\phi}\boldsymbol{\beta}(t) = \boldsymbol{\phi}^T\boldsymbol{\alpha}(t). \tag{61}$$

Finally, using (58) in (48), we obtain the new damage model:

$$[\overline{\mathbf{C}}(\boldsymbol{\beta})] = [\overline{\mathbf{C}}^0] - \tilde{\mathbf{C}} \cdot \boldsymbol{\Phi}\boldsymbol{\beta}, \tag{62}$$

which can also be written in tensor form as:

$$\overline{\mathbb{C}} = \overline{\mathbb{C}}^0 - \sum_{m=1}^{M} \hat{\mathbb{C}}^m \beta_m, \tag{63}$$

with

$$\hat{C}^m_{ijkl} = \sum_p \tilde{C}^p_{ijkl}\phi^p_m. \tag{64}$$

6.2 Thermodynamics

Using (64), the effective free energy of the material can be expressed by:

$$\overline{\omega} = \frac{1}{2}\overline{\boldsymbol{\varepsilon}} : \left[\overline{\mathbb{C}}^0 - \sum_{m=1}^{M} \hat{\mathbb{C}}^m \beta_m\right] : \overline{\boldsymbol{\varepsilon}}, \tag{65}$$

where $\overline{\boldsymbol{\varepsilon}}$ denotes the macroscopic strain tensor. From the Clausius-Duhem inequality, we have:

$$\overline{\omega} = \overline{\boldsymbol{\sigma}} : \dot{\boldsymbol{\varepsilon}} - \dot{\overline{\omega}}\left(\overline{\boldsymbol{\varepsilon}},\ \boldsymbol{\beta}\right) \geq 0. \tag{66}$$

where $\overline{\boldsymbol{\sigma}}$ is the macroscopic stress, expressed by:

$$\overline{\boldsymbol{\sigma}} = \frac{\partial \overline{\omega}}{\partial \boldsymbol{\varepsilon}} = \left[\overline{\mathbb{C}}^0 - \sum_{m=1}^{M} \hat{\mathbb{C}}^m \beta_m\right] : \overline{\boldsymbol{\varepsilon}} \tag{67}$$

and the rate of dissipated energy as

$$\overline{\phi} = \boldsymbol{\mathcal{A}} \cdot \boldsymbol{\beta} \geq 0, \tag{68}$$

where the components of the thermodynamic force vector $\boldsymbol{\mathcal{A}}$ associated with the flux vector $\dot{\boldsymbol{\beta}}$ take the remarkable simple form:

$$\mathcal{A}_k = -\frac{\partial \overline{\omega}}{\partial \beta_k} = \frac{1}{2}\overline{\boldsymbol{\varepsilon}} : \hat{\mathbb{C}}^k : \overline{\boldsymbol{\varepsilon}}. \tag{69}$$

7 New version of the DDHAD method: summary

7.1 Off-line calculations: data generation

- Compute $[\mathbf{C}^0]$.
- Apply P loads on the RVE for n^p load increments
  At each load increment t^p_n:

- Prescribe boundary conditions on the RVE and solve the crack propagation problem, e.g. using phase field method to fracture.
- Compute and store $\overline{\mathbb{C}}(t_n^p)$ by computational homogenization for $n = 1, 2, ..., n^p$, $p = 1, 2, ..., P$.

- For all pre-computed values of $\overline{\mathbb{C}}(t_n^p)$, compute the internal variables as described in section 3.2 and store them in a matrix $\mathbf{Q}$ as:
  - $\mathbf{Q} = \left[\boldsymbol{\alpha}(t_1^1), \boldsymbol{\alpha}(t_2^1), ..., \boldsymbol{\alpha}(t_{n^P}^P)\right]$.
  - Solve the eigenvalue problem $\mathbf{Q}\mathbf{Q}^T\boldsymbol{\phi}_k = \lambda_k\boldsymbol{\phi}_k$.
  - Select the M relevant eigenvectors from criterion (57) and store them in the matrix $\boldsymbol{\Phi} = [\boldsymbol{\phi}_1, \boldsymbol{\phi}_2, ..., \boldsymbol{\phi}_M]$.
  - Compute $\tilde{\mathbf{C}}$ from (49).

7.2 On-line calculations

At each load increment t_n^p, $p = 1, 2, ..., P^m$:

- Update internal variables $\boldsymbol{\beta}(t_n^p)$ from the macro mechanical fields at t_n^{p-1} (note that this point remains to be developed, and is reported to future studies).
- Given $\boldsymbol{\beta}(t_n^p)$, evaluate $[\overline{\mathbf{C}}(t_n^p)]$ by

$$[\overline{\mathbf{C}}(t_n^p)] = [\overline{\mathbf{C}}^0] - \tilde{\mathbf{C}} \cdot \boldsymbol{\Phi}\boldsymbol{\beta}(t_n^p).$$

- Solve the mechanical problem $\nabla \cdot \big(\overline{\mathbb{C}}(t_n^p) : \overline{\boldsymbol{\varepsilon}}\big) + \overline{\mathbf{b}} = 0 \;\text{ in } \overline{\Omega}$.

8 Numerical examples

In this section, the proposed method is applied to a 3D RVE problem, as validation test. An RVE associated with a 3D printed lattice structure is considered, whose geometry is depicted in Fig. 2 (a)-(b). The lattice corresponds to a body-centered cubic lattice. The length of one side of the RVE is $L = 1$ mm. The lateral bars have square section of width $h = 0.1$ mm and the central bars have circular sections with diameters $D = 0.1$ mm. The RVE is composed of $2 \times 2 \times 2$ unit cells. The corresponding mesh contains 192,000 tetrahedral elements, and is depicted in Fig. 2 (c).

Off-line calculations consist of 3 simulations where the load is applied along each of the principal directions of the 3D frame. More specifically, KUBC boundary conditions $\mathbf{u}(\mathbf{x}) = \overline{\boldsymbol{\varepsilon}}\mathbf{x}$ (see e.g. [40]) are prescribed on the boundary $\partial\Omega$ of the RVE, where $\mathbf{u}$ denotes the displacement vector, $\mathbf{x}$ is the position vector, and $\overline{\boldsymbol{\varepsilon}}$ is a macroscopic strain. Three loads are applied independently along the basis vectors $\mathbf{n}_1 = \mathbf{e}_1$, $\mathbf{n}_2 = \mathbf{e}_2$ and $\mathbf{n}_3 = \mathbf{e}_3$, corresponding to the macroscopic strain fields

$$\overline{\boldsymbol{\varepsilon}}^1 = \begin{bmatrix} \epsilon & 0 & 0 \\ 0 & 0 & 0 \\ 0 & 0 & 0 \end{bmatrix}, \overline{\boldsymbol{\varepsilon}}^2 = \begin{bmatrix} 0 & 0 & 0 \\ 0 & \epsilon & 0 \\ 0 & 0 & 0 \end{bmatrix}, \overline{\boldsymbol{\varepsilon}}^3 = \begin{bmatrix} 0 & 0 & 0 \\ 0 & 0 & 0 \\ 0 & 0 & \epsilon \end{bmatrix}, \tag{70}$$

respectively (see Fig. 2 (b), where ϵ is a loading parameter. The material parameters are $E = 52$ GPa, $\sigma_c = 3$ Mpa, $\nu = 0.3$, $\psi^c = \sigma_c^2/(2E)$ (see e.g. [54] for a detailed description of the phase field fracture model and numerical implementation used here), where E denotes Young's modulus, ν is Poisson's ratio, σ_c is the critical fracture stress and ψ^c is a specific fracture energy per unit volume. The regularization parameter is taken as $\ell = 0.04$ mm. Along each direction, 60 strain load steps $\Delta\epsilon = 2.5 \times 10^{-6}$ are adopted.

The on-line calculations are conducted along three loads, denoted by load A, load B and load C, respectively. Load A is a monotonic load corresponding to a strain prescribed along a normal vector $\mathbf{n}^A = \{\sqrt{3}/2, 1/2, 0\}$, forming an angle $\theta = \pi/6$ with the x-axis in the $x-y$ plane. The corresponding strain tensor $\overline{\boldsymbol{\varepsilon}}^A = \epsilon\mathbf{n}^A \otimes \mathbf{n}^A$ is given by

$$\overline{\boldsymbol{\varepsilon}}^A(\epsilon) = \epsilon \times \begin{bmatrix} 3/4 & \sqrt{(3)}/4 & 0 \\ \sqrt{(3)}/4 & 1/4 & 0 \\ 0 & 0 & 0 \end{bmatrix} \tag{71}$$

where ϵ is a loading parameter. The load is prescribed by 60 load increments $\Delta\epsilon = 2.5 \times 10^{-6}$. Load B is a more complex load, where the following strain states are reached successively: (i) a 11− traction strain; (ii), combining 11− traction and 12− shear strains; (iii) combining 11−, 33− traction and 12− shear strains, and finally a 11− compressive strain. A linear interpolation is performed between the different strain states, starting from zero strain. Each step consists of 15 load increments $\Delta\epsilon = 2.5 \times 10^{-6}$. The different strain states are summmarized as follows for load B.

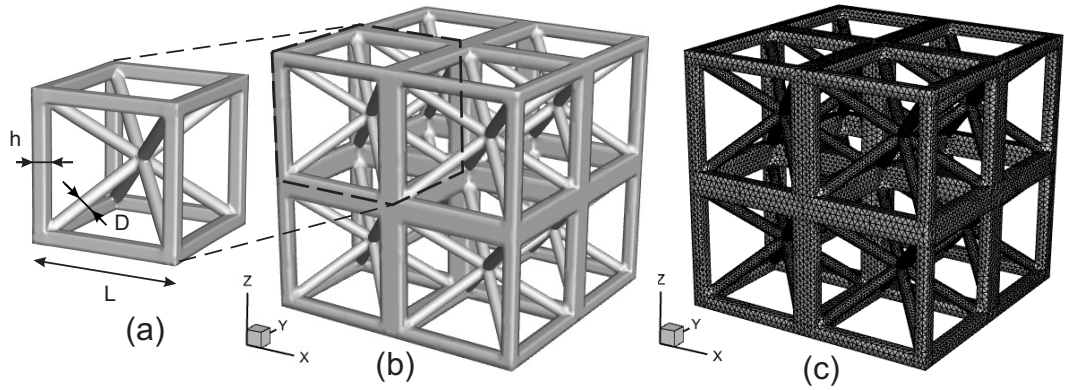

Fig. 2 (a) Unit cell defining the lattice structure; (b) RVE composed of $2 \times 2 \times 2$ unit cells; (c) corresponding mesh.

$$\begin{bmatrix} 0 & 0 & 0 \\ 0 & 0 & 0 \\ 0 & 0 & 0 \end{bmatrix} \rightarrow \underbrace{\begin{bmatrix} 0.6 & 0 & 0 \\ 0 & 0 & 0 \\ 0 & 0 & 0 \end{bmatrix}}_{11-traction} \rightarrow \underbrace{\begin{bmatrix} 0.6 & 0.2 & 0 \\ 0.2 & 0 & 0 \\ 0 & 0 & 0 \end{bmatrix}}_{11-traction+12-shear}$$

$$\rightarrow \underbrace{\begin{bmatrix} 0.6 & 0.2 & 0 \\ 0.2 & 0 & 0 \\ 0 & 0 & 0.4 \end{bmatrix}}_{11\ +33-traction+12-shear} \rightarrow \underbrace{\begin{bmatrix} -0.3 & 0 & 0 \\ 0 & 0 & 0 \\ 0 & 0 & 0 \end{bmatrix}}_{11-Compression} \tag{72}$$

Similarly, Load C also consists of several steps which are described as follows.

$$\begin{bmatrix} 0 & 0 & 0 \\ 0 & 0 & 0 \\ 0 & 0 & 0 \end{bmatrix} \rightarrow \underbrace{\begin{bmatrix} -0.6 & 0 & 0 \\ 0 & 0 & 0 \\ 0 & 0 & 0 \end{bmatrix}}_{11-compression}$$

$$\rightarrow \underbrace{\begin{bmatrix} -0.6 & 0 & 0 \\ 0 & 0 & 0 \\ 0 & 0 & 0.8 \end{bmatrix}}_{11-compress.+33-tract.} \rightarrow \underbrace{\begin{bmatrix} -0.6 & 0.3 & 0 \\ 0.3 & 0 & 0 \\ 0 & 0 & 0.8 \end{bmatrix}}_{11-compress.+33-tract.+12-shear} \tag{73}$$

The first two steps consist of 15 load increments and the last step consists of 30 load increments. All increments have the value $\Delta\epsilon = 2.5 \times 10^{-6}$.

The evolutions of the 21 internal variables based on the Fourier series defined in Appendix C during the off-line calculations are depicted in Fig. 3, where the evolutions corresponding to the 3 off-line loads are grouped in the same figure. During the off-line stage, the matrices $\overline{\mathbf{C}}^0$, $\tilde{\mathbf{C}}$ and the reduced basis $\mathbf{\Phi}$ (see Eq. (58)) are also computed based on these 3 loads. The evolutions of the 21 internal variables relative to the 3 loads are grouped in a matrix $\mathbf{Q}$ and the POD defined in section 6 is applied. The evolutions of the eigenvalues are depicted in Fig. 4. We note that the eigenvalues quickly drop, indicating that only a few basis vectors are necessary to represent the evolution of the whole set of internal variables. For all 3 loads A, B and C, the approximation of the effective elasticity tensor $\overline{\mathbb{C}}$ using the approximation from the Fourier series in (48) is evaluated. For this purpose, several values N of internal variables contained in the vector $\boldsymbol{\alpha}$ (see Eqs. (C45)-(C52)) are used to evaluate the accuracy of the DDHAD approximation. Second, the approximation of $\overline{\mathbb{C}}$ using the reduced variables in Eq. (62) is evaluated by keeping only M basis vectors in $\mathbf{\Phi}$ (see section 6.1). In the different examples, only a limited number of components are depicted, for the sake of clarity. Note that in this work, the evolution law for the reduced variables $\boldsymbol{\beta}$ is not studied. To obtain a reference solution, we proceed as follows: (i) the evolution of the reference effective elastic tensor $\overline{\mathbb{C}}(t)$ is evaluated by DNS (Direct Numerical Simulation) using the computational homogenization framework described in section 2; (ii) given $\overline{\mathbb{C}}(t)$, the Fourier-based internal variables $\boldsymbol{\alpha}(t)$ are extracted using the procedure described in subsection 3.1; (iii) finally, the reduced internal variables $\boldsymbol{\beta}(t)$ are obtained by the procedure described in section 6.1, by solving (61).

For illustration, the damage in the RVE at the end of Loads A, B and C is depicted in Fig. 5.

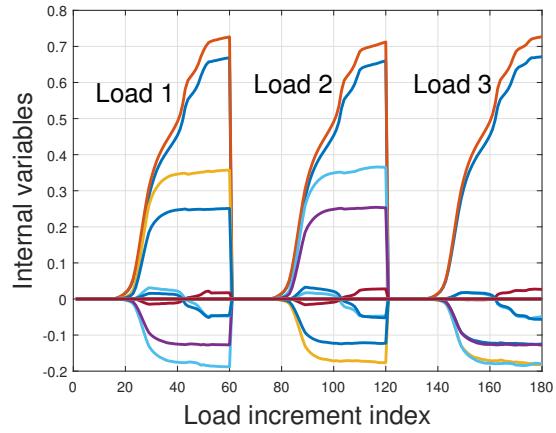

Fig. 3 Evolution of Fourier Series internal variables during the off-line calculations.

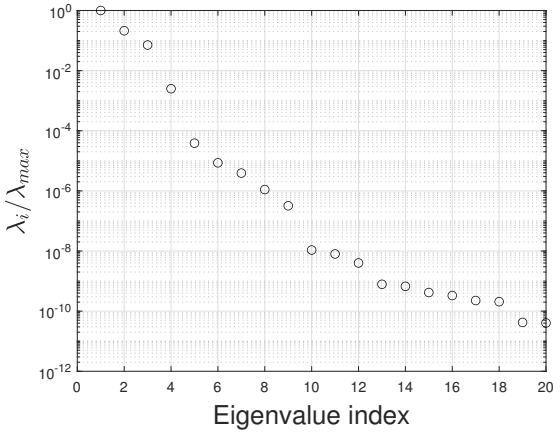

Fig. 4 Eigenvalues associated with the reduced basis vectors, with $\lambda_{max} = max(\lambda_i)$.

Results are presented in Fig. 6 for the DDHAD model using the Fourier-based internal variables (48) along load A. We can note that to obtain a very accurate representation of all components during the whole loading, at least 10 internal variables are required, even though $N = 8$ internal variables provides a reasonable approximation.

In Fig. 7 the DDHAD model (62) using the reduced internal variables is evaluated for Load A. It can be clearly observed that much less internal variables are required for this model to reproduce the reference solution. As $M = 3$ internal variables allow a very accurate representation of the reference solution, keeping only $M = 2$ still provides a reasonable approximation. We remind that the present load A, like loads B and C, are new loads, not seen during the off-line stage.

The solution obtained by the DDHDAD damage model using Fourier-based internal variables is despicted in Fig. 8 for Load B. Here again, we can note that between 8 and 10 internal variables are needed here to obtain an accurate solution as compared to DNS. The DDHAD model solution using reduced internal variables is depicted in Fig. 9. Remarkably, only 3 internal variables are again sufficient to represent the induced anisotropy of the elastic tensor in this new configuration, involving complex loading, not seen during ther off-line stage.

Results for Load C are presented in Figs. 10 and 11 for Fourier-based internal variables and reduced variables DDHAD solutions. Similar conclusions can be established as previsously.

For evaluation of integrals in (C28)-(C32), it was found that a uniform discretization of the angular space $[0, \pi] \times [0, 2\pi]$ into 50×100 integration points was sufficient to reach convergence in the approximation of the effective elasticity tensor evolution. For this discretization, even though the integral calculations are fast, using the precomputed operators as described in Appendix D allows a computational gain ratio of about 20 as compared to the original version of the method.

To conclude, the above examples show that: (i) The DDHAD model involving Fourier-series based internal variables is very accurate, but may require a large number if internal variables in 3D (typically between 8 and 10) to describe the damage of the elastic tensor along complex loads; (ii) the DDHAD model with reduced internal variables requires much less internal variables, and is capable of providing accurate solutions with a few number of internal variables (typically 3 in 3D), and using a few off-line simulations (here three loads along the main directions), even if the on-line simulations involve complex loads, such as combined multi-axial traction, shear or compression.

9 Conclusion

A modified version of the so-called DDHAD method (Data-Driven Harmonic Analysis of Damage) has been proposed. The original version of this method uses crack numerical simulations on Representative Volume Elements (RVE) as data

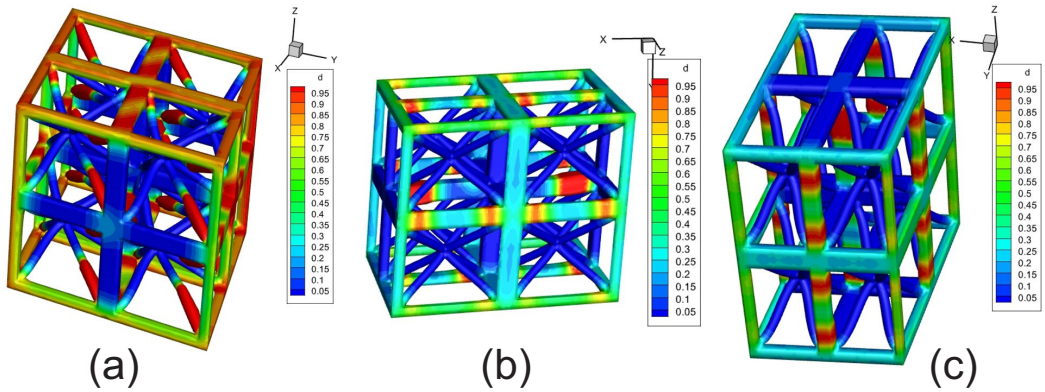

Fig. 5 Damage field in the RVE at the end of the on-line Loads A, B and C, (a), (b) and (c) respectively. Exaggerated deformations are depicted.

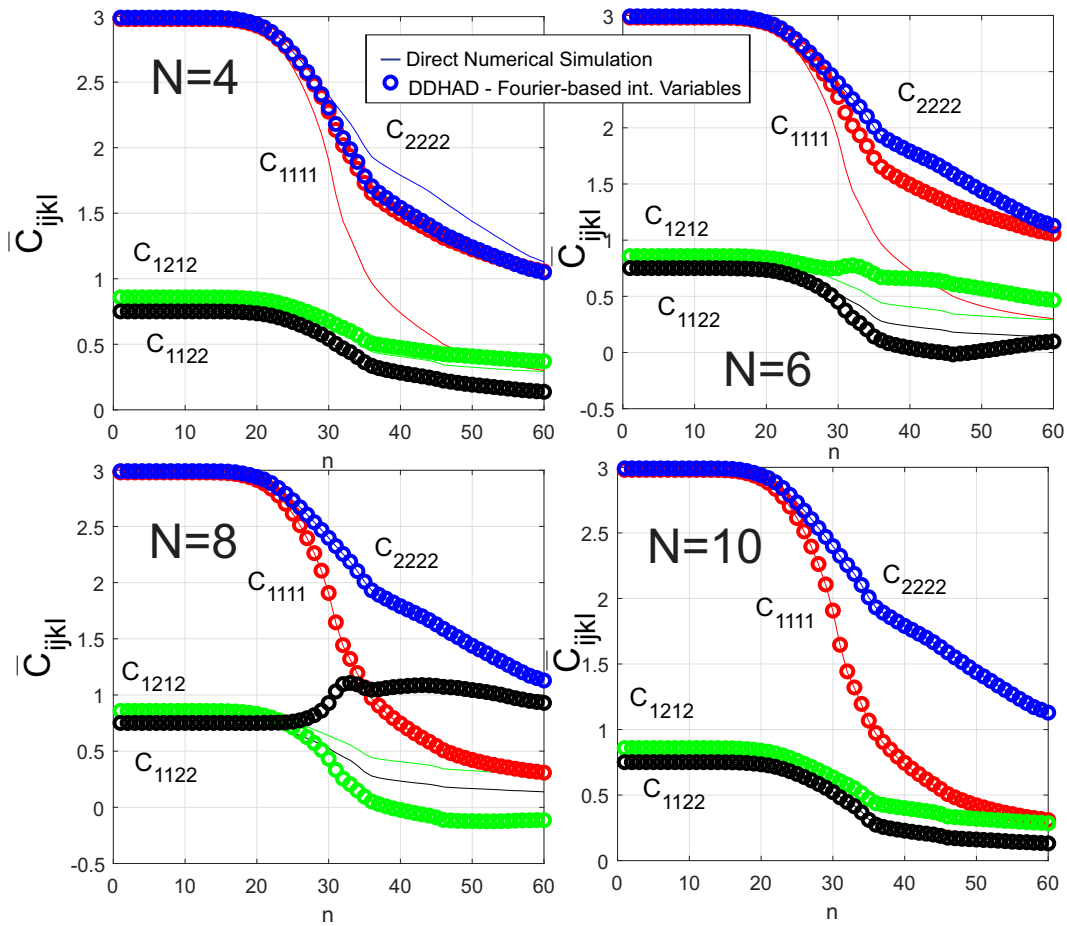

Fig. 6 Damage of the elasticity tensor components associated with the RVE in Fig. 2 along Load A. Comparison between Direct Numerical Simulation (reference) and the DDHAD model, using Fourier-based definition of internal variables and different numbers N of terms in the Fourier series.

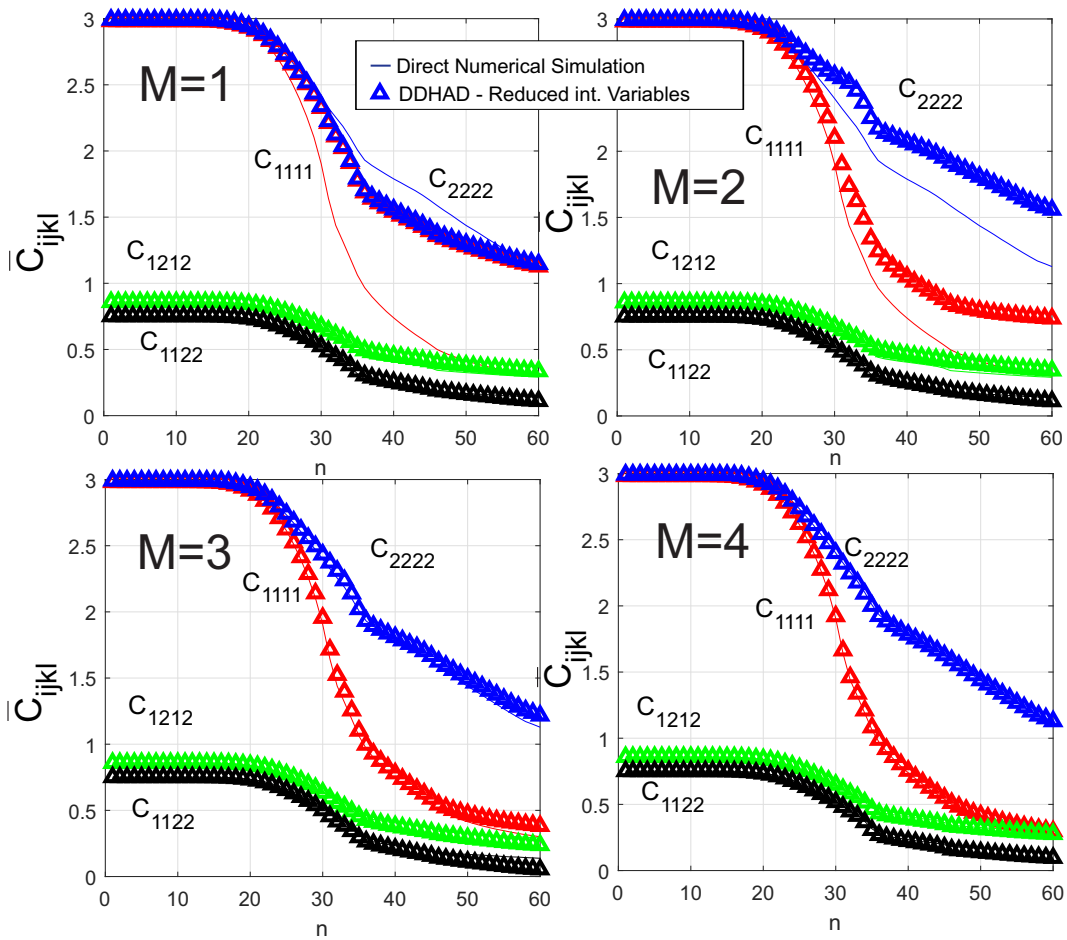

Fig. 7 Damage of the elasticity tensor components associated with the RVE in Fig. 2 along Load A. Comparison between Direct Numerical Simulation (reference) and the DDHAD model, using reduced internal variables and different numbers M of terms in the POD approximation.

to construct an anisotropic damage model for the corresponding homogenized material. A harmonic analysis-based damage model, employing two Orientation Distribution Functions (ODFs) to describe the anisotropic damage evolution, are identified from the simulation data. The damage ODFs are parametrized using spherical harmonics. In the new version proposed in this paper, two improvements have been proposed. First, the computational costs related to the integrals calculations arising from the Fourier series are drastically reduced by using pre-computed operators. Second, a Reduced Order Model technique based on Proper Orthogonal Decomposition (POD) is applied to reduce the number of internal variables in the formulation. As a result, a compact and simple form of the damage model, able to describe both initial and induced damage anisotropies, is provided. The proposed approach has been applied to a 3D RVE of a 3D printed lattice structure, exhibiting a strong induced anisotropy. It was shown that the harmonic analysis-based damage model requires a large number of internal variables due to the strong induced anisotropy of the microstructure during its damage. In contrast, the proposed model with reduced internal variables only requires a few internal variables (about 3) for a comparable accuracy. The development of evolution laws for the internal variables in this context remains to be done and will be the topic of a forthcoming study.

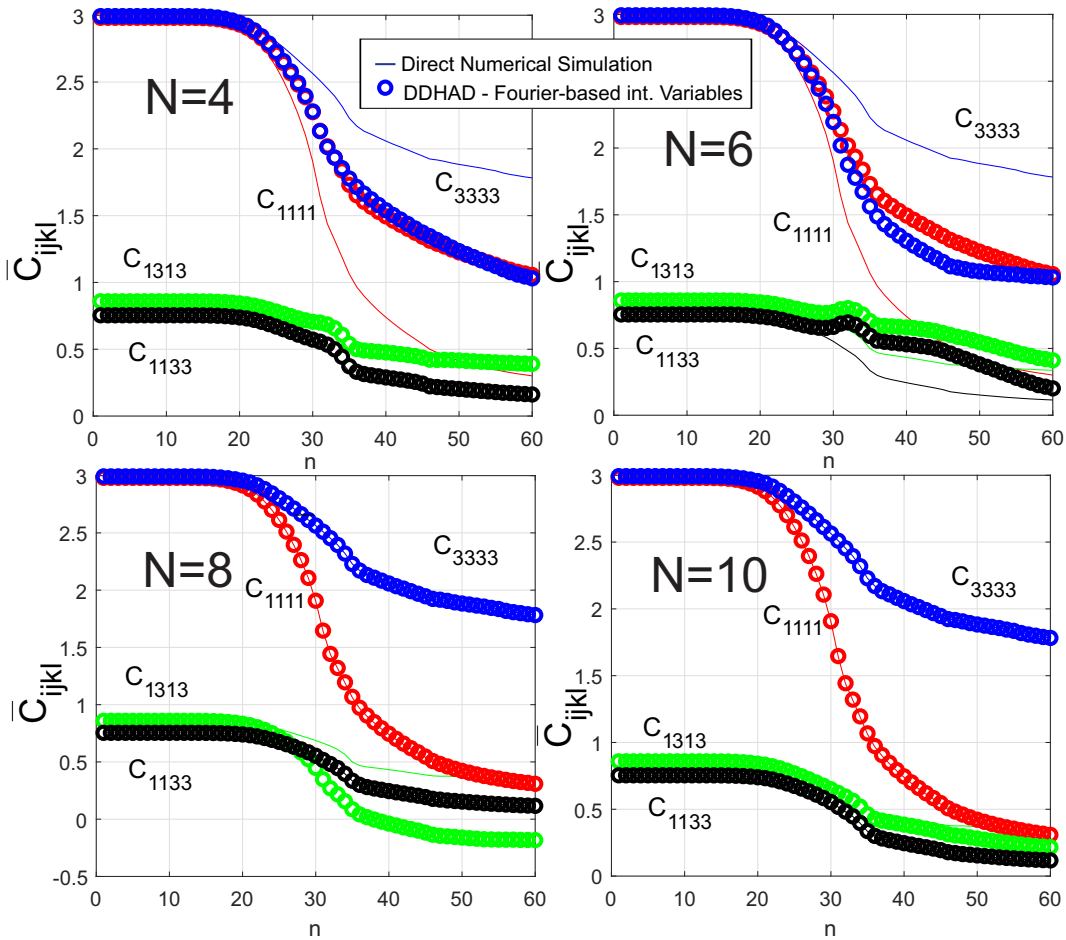

Fig. 8 Damage of the elasticity tensor components associated with the RVE in Fig. 2 along Load B. Comparison between Direct Numerical Simulation (reference) and the DDHAD model, using Fourier-based definition of internal variables and different numbers N of terms in the Fourier series.

Appendix A Appendix: Generalized harmonics

In (20), $\{1, \mathbf{F}, \mathbb{F}\}$ forms a complete orthogonal basis for square-integrable functions on $\mathcal{S}$. Note that the orthogonality of the basis functions $\{1, \mathbf{F}, \mathbb{F}\}$ implies that

$$\int_{\mathcal{S}} \mathbf{F} dS = \mathbf{0}, \quad \int_{\mathcal{S}} \mathbb{F} dS = \mathbb{O}, \tag{A1}$$

$$\int_{\mathcal{S}} \mathbf{F} \otimes \mathbb{F} dS = \int_{\mathcal{S}} \mathbb{F} \otimes \mathbf{F} dS = \mathbb{O}_6 \tag{A2}$$

where $dS = d\theta$ in 2D and $dS = sin(\theta) d\theta d\varphi$ in 3D, where θ and φ denote the Euler angle in a spherical frame (see Fig. 1 (d)). Above, $\mathbb{O}_6$ represents the sixth-order zero tensor. Additionally, $\mathbf{F}$ is symmetric and traceless (ST), i.e.

$$\mathbf{F}^T = \mathbf{F}, \quad Tr(\mathbf{F}) = 0, \tag{A3}$$

and $\mathbf{F}$ is completely symmetric and traceless (CST), i.e.

$$\mathbb{F}_{ijkl} = \mathbb{F}_{jikl} = \mathbb{F}_{klij} = \mathbb{F}_{ikjl} \tag{A4}$$

and

$$\mathbb{F}_{ijkk} = 0. \tag{A5}$$

A.1 2D case

In 2D,

$$n_1 = cos(\theta), \quad n_2 = sin(\theta), \tag{A6}$$

and

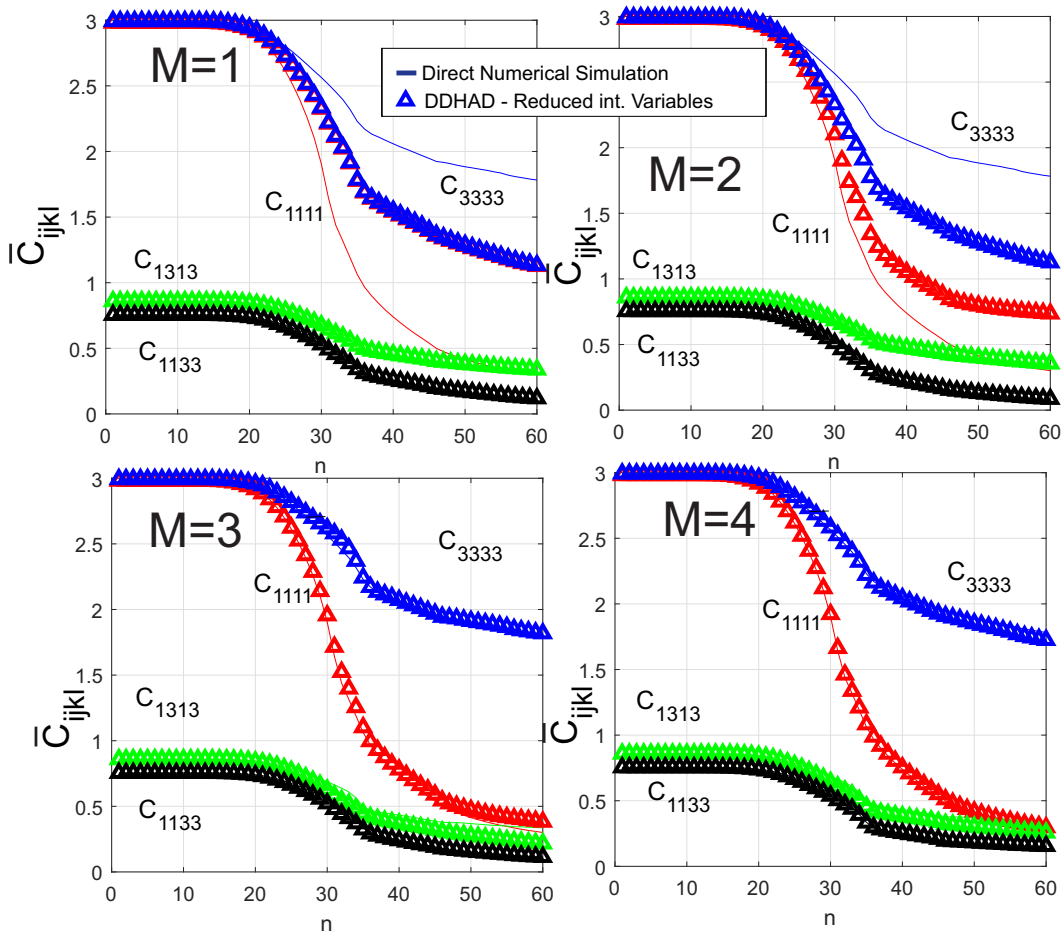

Fig. 9 Damage of the elasticity tensor components associated with the RVE in Fig. 2 along Load B. Comparison between Direct Numerical Simulation (reference) and the DDHAD model, using reduced internal variables and different numbers M of terms in the POD approximation.

$$\mathbf{F}(\theta) = \mathbf{N} - \frac{1}{2}\mathbf{I}. \tag{A7}$$

The fourth-order tensor $\mathbb{F}$ is given in 2D as [27]

$$\mathbb{F}_{ijkl}(\theta) = n_i n_j n_k n_l$$

$$-\frac{1}{6}\left(\delta_{ij}n_k n_l + n_i n_j \delta_{kl} + \delta_{ik}n_j n_l + \delta_{il}n_j n_k\right.$$

$$\left.+n_{ik}\delta_{jl} + n_i n_l \delta_{jk}\right)$$

$$+\frac{1}{24}\left(\delta_{ij}\delta_{kl} + \delta_{ik}\delta_{jl} + \delta_{il}\delta_{jk}\right). \tag{A8}$$

A.2 3D case

In 3D, the components of the normal to the unit sphere are expressed as a function of the Euler angles θ and φ in a spherical frame (see Fig. 1 (d)) according to

$$n1 = sin(\theta)cos(\varphi), \quad n2 = sin(\theta)sin(\varphi),$$

$$n3 = cos(\theta), \tag{A9}$$

$$\mathbf{F}(\theta,\varphi) = \mathbf{N} - \frac{1}{3}\mathbf{I}, \tag{A10}$$

and the fourth-order tensor $\mathbb{F}$ is given by (see e.g. [26])

$$\mathbb{F}_{ijkl}(\theta,\varphi) = N_{ij}N_{kl}$$

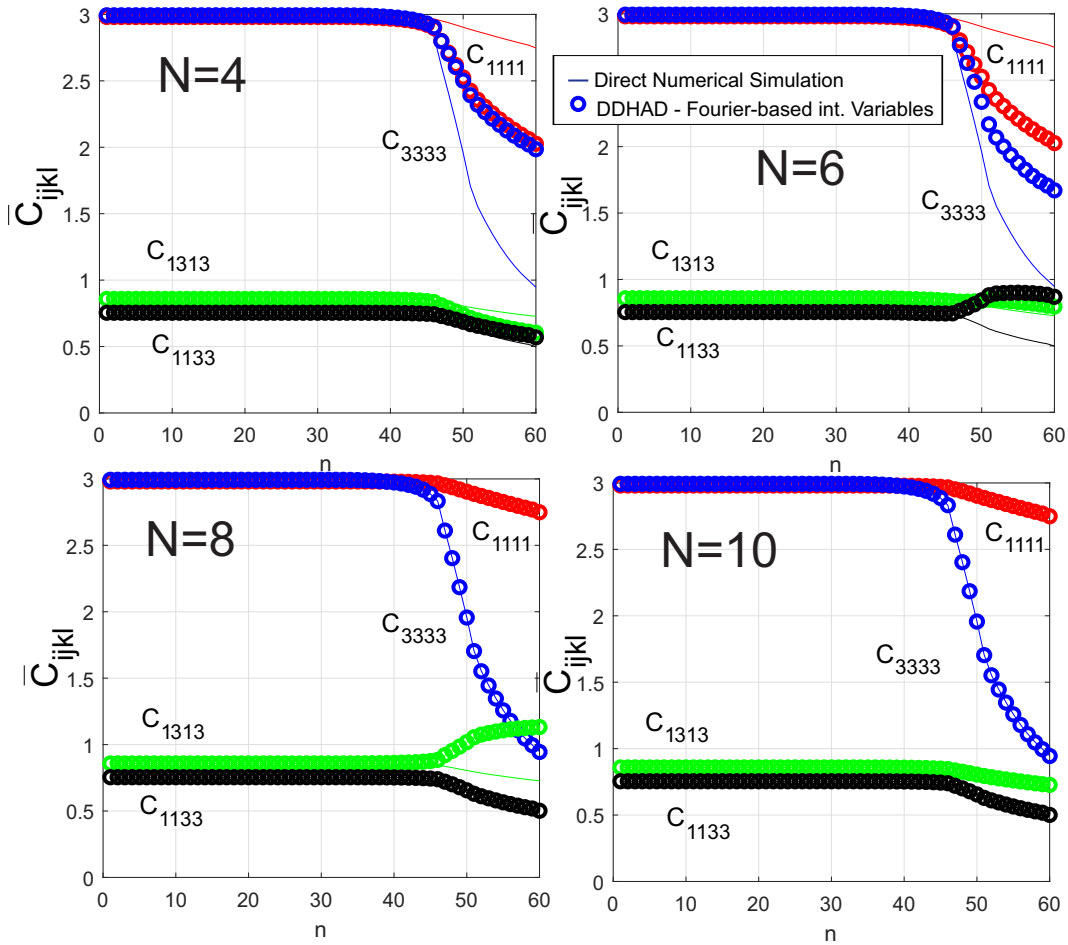

Fig. 10 Damage of the elasticity tensor components associated with the RVE in Fig. 2 along Load C. Comparison between Direct Numerical Simulation (reference) and the DDHAD model, using Fourier-based definition of internal variables and different numbers N of terms in the Fourier series.

$$-\frac{1}{7}\left(\delta_{ij}N_{kl}+N_{ij}\delta_{kl}+\delta_{il}N_{jk}\right.$$

$$\left.+N_{il}\delta_{jk}+\delta_{ik}N_{jl}+N_{ik}\delta_{jl}\right)$$

$$+\frac{1}{35}\left(\delta_{ij}\delta_{kl}+\delta_{il}\delta_{jk}+\delta_{ik}\delta_{jl}\right). \qquad \text{(A11)}$$

Appendix B Appendix: Reconstruction of the 3D stiffness tensor from orientation functions

In 3D, the orientation functions can be parameterized by two Euler angles $\theta \in [0;\ \pi]$, $\varphi \in [0;\ 2\pi]$ (see Fig. 1 (d)), then $\eta(\mathbf{n}) \equiv \eta(\theta,\varphi)$, $\kappa(\mathbf{n}) \equiv \kappa(\theta,\varphi)$. The irreducible form of the elasticity tensor is in that case given by [42, 43, 48]:

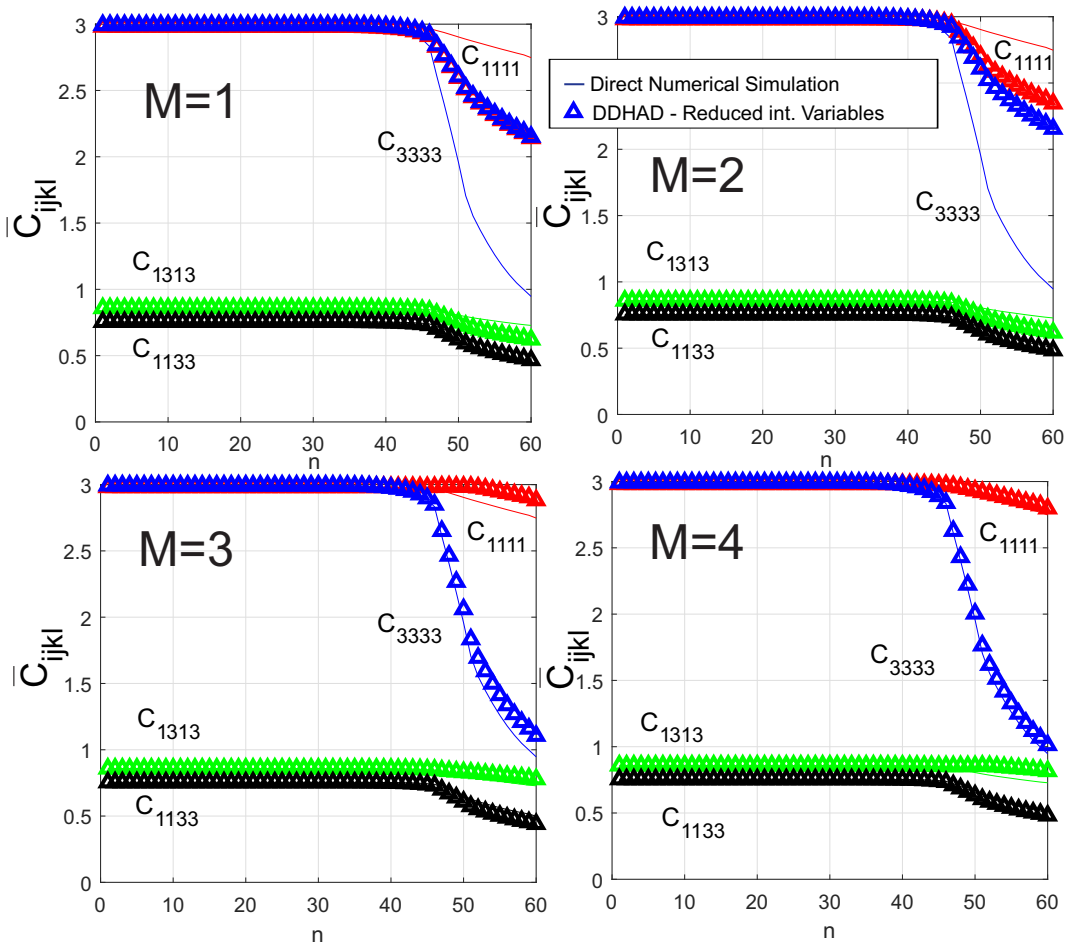

Fig. 11 Damage of the elasticity tensor components associated with the RVE in Fig. 2 along Load C. Comparison between Direct Numerical Simulation (reference) and the DDHAD model, using reduced internal variables and different numbers M of terms in the POD approximation.

$$\mathbb{C} = \lambda \mathbf{I}\otimes\mathbf{I} + \mu \mathbf{I}\underline{\otimes}\mathbf{I} + \mathbf{I}\otimes\mathbf{A} + \mathbf{A}\otimes\mathbf{I} + \mathbf{I}\underline{\otimes}\mathbf{B} + \mathbf{B}\underline{\otimes}\mathbf{I} + \mathbb{Z}, \tag{B12}$$

where λ and μ are the Lamé's coefficients, $\mathbf{A}$ and $\mathbf{B}$ are second-order tensors and $\mathbb{Z}$ is a fourth-order tensor. In the 3D case, theses different quantities can be related to the orientation functions $\eta(\theta,\phi)$ and $\kappa(\theta,\phi)$ as follows [26]:

$$\alpha = \frac{1}{2}(b-a), \quad \beta = \frac{1}{4}(3a-b), \tag{B13}$$

$$\mathbf{A} = \mathbf{V} - \mathbf{U}, \quad \mathbf{B} = \frac{1}{4}\left(3\mathbf{U} - 2\mathbf{V}\right), \tag{B14}$$

$$a = \frac{1}{4\pi}\int_{\theta=0}^{\pi}\int_{\varphi=0}^{2\pi} \eta(\theta,\varphi) sin(\theta) d\theta d\varphi, \tag{B15}$$

$$b = \frac{1}{4\pi}\int_{\theta=0}^{\pi}\int_{\varphi=0}^{2\pi} \kappa(\theta,\varphi) sin(\theta) d\theta d\varphi, \tag{B16}$$

$$\mathbf{U} = \frac{15}{8\pi}\int_{\theta=0}^{\pi}\int_{\varphi=0}^{2\pi} \mathbf{F}(\theta,\varphi)\eta(\theta,\varphi) sin(\theta) d\theta d\varphi, \tag{B17}$$

$$\mathbf{V} = \frac{15}{8\pi}\int_{\theta=0}^{\pi}\int_{\varphi=0}^{2\pi}\mathbf{F}(\theta,\varphi)\kappa(\theta,\varphi)sin(\theta)d\theta d\varphi, \tag{B18}$$

$$\mathbb{Z} = \frac{315}{32\pi}\int_{\theta=0}^{\pi}\int_{\varphi=0}^{2\pi}\mathbb{F}(\theta,\varphi)\eta(\theta,\varphi)sin(\theta)d\theta d\varphi. \tag{B19}$$

A convenient matrix form of the elasticity tensor is introduced as

$$\overline{\mathbf{C}} = \alpha\mathbf{I}^1 + \beta\mathbf{I}^2 + \overline{\mathbf{A}} + \overline{\mathbf{B}} + \mathbf{Z} \tag{B20}$$

with

$$\mathbf{I}^1 = \begin{bmatrix} 1&1&1&0&0&0\\ 1&1&1&0&0&0\\ 1&1&1&0&0&0\\ 0&0&0&0&0&0\\ 0&0&0&0&0&0\\ 0&0&0&0&0&0 \end{bmatrix}, \quad \mathbf{I}^2 = \begin{bmatrix} 2&0&0&0&0&0\\ 0&2&0&0&0&0\\ 0&0&2&0&0&0\\ 0&0&0&1&0&0\\ 0&0&0&0&1&0\\ 0&0&0&0&0&1 \end{bmatrix}, \tag{B21}$$

$$\overline{\mathbf{A}} = \begin{bmatrix} 2A_{11} & (A_{11}+A_{22}) & (A_{11}+A_{33}) & A_{12} & A_{13} & A_{23}\\ & 2A_{22} & (A_{22}+A_{33}) & A_{12} & A_{13} & A_{23}\\ & & 2A_{33} & A_{12} & A_{13} & A_{23}\\ & & & 0 & 0 & 0\\ & & & & 0 & 0\\ Sym. & & & & & 0 \end{bmatrix}, \tag{B22}$$

and

$$\overline{\mathbf{B}} = \begin{bmatrix} 4B_{11} & 0 & 0\\ & 4B_{22} & 0\\ & & 4B_{33}\\ & & \\ & & \\ Sym. & & \end{bmatrix}$$

$$\begin{bmatrix} 2B_{12} & 2B_{13} & 0\\ & 0 & 2B_{23}\\ 0 & 2B_{13} & 2B_{23}\\ (B_{11}+B_{22}) & B_{23} & B_{13}\\ & (B_{11}+B_{22}) & B_{12}\\ & & (B_{22}+B_{33}) \end{bmatrix}, \tag{B23}$$

and $\mathbf{Z}$ is the matrix form associated with $\mathbb{Z}$ and is computed by

$$\mathbf{Z} = \frac{315}{32\pi}\int_{\theta=0}^{\pi}\int_{\varphi=0}^{2\pi}\hat{\mathbf{F}}(\theta,\varphi)\eta(\theta,\varphi)sin(\theta)d\theta d\varphi. \tag{B24}$$

with

$$\hat{\mathbf{F}}(\theta,\phi) = \begin{bmatrix} F_{1111} & F_{1122} & F_{1133} & F_{1112} & F_{1113} & F_{1123}\\ & F_{2222} & F_{2233} & F_{2212} & F_{2213} & F_{2223}\\ & & F_{3333} & F_{3312} & F_{3313} & F_{3323}\\ & & & F_{1212} & F_{1213} & F_{1223}\\ & & & & F_{1313} & F_{1323}\\ Sym. & & & & & F_{2323} \end{bmatrix}. \tag{B25}$$

Appendix C Appendix: 3D formulation of harmonic analysis-based damage model

Similarly, at each time step t, $d(\theta,\varphi,t)$ and $h(\theta,\varphi,t)$ can be computed through (17) and are expanded according to

$$d(\theta,\varphi) \simeq d_0 + \mathbf{D} : \mathbf{F}(\theta,\varphi) + \mathbb{D} :: \mathbb{F}(\theta,\varphi), \tag{C26}$$

$$h(\theta,\varphi) \simeq h_0 + \mathbf{H} : \mathbf{F}(\theta,\varphi), \tag{C27}$$

where

$$d_0 = \frac{1}{4\pi}\int_{\theta=0}^{\pi}\int_{\varphi=0}^{2\pi}d(\theta,\varphi)sin(\theta)d\theta d\varphi, \tag{C28}$$

$$h_0 = \frac{1}{4\pi}\int_{\theta=0}^{\pi}\int_{\varphi=0}^{2\pi}h(\theta,\varphi)sin(\theta)d\theta d\varphi, \tag{C29}$$

$$\mathbf{D} = \frac{15}{8\pi}\int_{\theta=0}^{\pi}\int_{\varphi=0}^{2\pi}d(\theta,\varphi)\mathbf{F}(\theta,\varphi)sin(\theta)d\theta d\varphi, \tag{C30}$$

$$\mathbf{H} = \frac{15}{8\pi}\int_{\theta=0}^{\pi}\int_{\varphi=0}^{2\pi} h(\theta,\varphi)\mathbf{F}(\theta,\varphi)sin(\theta)d\theta d\varphi. \tag{C31}$$

and

$$\mathbb{D} = \frac{315}{32\pi}\int_{\theta=0}^{\pi}\int_{\varphi=0}^{2\pi} d(\theta,\varphi)\mathbb{F}(\theta,\varphi)sin(\theta)d\theta d\varphi. \tag{C32}$$

For a given time t, $\eta(\theta,\varphi,t)$ and $\kappa(\theta,\varphi,t)$ can be reconstructed according to (21)-(22) and (C26)-(C27) and the elasticity tensor can be reconstructed by (B12)-(B19).

Here again, because of the symmetry properties of the different tensors, a maximum of 21 internal variables can be defined as follows.

The tensors $\mathbf{D}$ and $\mathbf{H}$ are traceless. Then,

$$D_{ii} = 0, \quad H_{ii} = 0. \tag{C33}$$

The tensors $\mathbf{D}$ and $\mathbf{H}$ then contain 10 independent constants. As $\mathbb{D}$ is completely symmetric, then

$$D_{ijkl} = D_{jikl} = D_{ikjl} = D_{ijlk}. \tag{C34}$$

This allows establishing the relationships

$$D_{1212} = D_{1122}, \quad D_{1213} = D_{1123}, \tag{C35}$$

$$D_{1223} = D_{2213}, \quad D_{1313} = D_{1133}, \tag{C36}$$

$$D_{1323} = D_{3312}, \quad D_{2323} = D_{2233}. \tag{C37}$$

Then 6 constants can be eliminated amongst the 21 ones contained in $\mathbb{D}$. In addition, $\mathbb{D}$ is traceless, then:

$$D_{iikl} = 0, \tag{C38}$$

which allows eliminating 6 additional constants according to

$$D_{3312} = -D_{1112} - D_{2212}, \tag{C39}$$

$$D_{3313} = -D_{1113} - D_{2213}, \tag{C40}$$

$$D_{3323} = -D_{1123} - D_{2223}, \tag{C41}$$

$$D_{1133} = -D_{1111} - D_{1122}, \tag{C42}$$

$$D_{2233} = -D_{1122} - D_{2222}, \tag{C43}$$

$$D_{3333} = D_{1111} + D_{2222} + 2D_{1122}. \tag{C44}$$

Then, $\mathbb{D}$ can be expressed using only 9 independent constants which are added to the set of internal variables. Finally, a maximum of 21 constants is sufficient to fully define the damage of an arbitrary 3D anisotropic medium. Note that in practice, this number can be much lower, as some internal variables may not play a role, as shown in [37]. For the sake of clarity, we re-name the 21 internal variables as

$$\alpha_1 = d_0, \quad \alpha_2 = h_0, \tag{C45}$$

$$\alpha_3 = D_{11}, \quad \alpha_4 = D_{12}, \quad \alpha_5 = D_{13}, \tag{C46}$$

$$\alpha_6 = D_{22}, \quad \alpha_7 = D_{23}, \tag{C47}$$

$$\alpha_8 = H_{11}, \quad \alpha_9 = H_{12}, \quad \alpha_{10} = H_{13}, \tag{C48}$$

$$\alpha_{11} = H_{22}, \quad \alpha_{12} = H_{23}, \tag{C49}$$

$$\alpha_{13} = D_{1111}, \quad \alpha_{14} = D_{1122}, \quad \alpha_{15} = D_{2222}, \tag{C50}$$

$$\alpha_{16} = D_{1112}, \quad \alpha_{17} = D_{1113}, \quad \alpha_{18} = D_{1123}, \tag{C51}$$

$$\alpha_{19} = D_{2212}, \quad \alpha_{20} = D_{2213}, \quad \alpha_{21} = D_{2223}. \tag{C52}$$

Note that as $\mathbb{Z}$ is completely symmetric and traceless, the same relationships between the components of $\mathbb{Z}$ and the above ones for $\mathbb{D}$ hold, i.e. Eq. (C36)-(C44) can be used by just replacing D_{ijkl} by Z_{ijkl}.

Appendix D Appendix: Fast evaluation of the elasticity tensor in the 3D case

Using the definition (C26) and (C27), the compact form (34) can be adopted with $\boldsymbol{\alpha}^T = [\alpha_1, \alpha_2, ..., \alpha_{21}]$, then $\mathbf{V}^d$ and $\mathbf{V}^h$ are defined as follows. To alleviate the notations, we ommit the dependence of θ and φ if no confusion is possible:

$$\mathbf{V}^d = \begin{bmatrix} 1 \\ 0 \\ F_{11} - F_{33} \\ 2F_{12} \\ 2F_{13} \\ F_{22} - F_{33} \\ 2F_{23} \\ 0 \\ 0 \\ 0 \\ 0 \\ 0 \\ F_{1111} + F_{3333} - 2F_{1133} - 4F_{1313} \\ (2F_{3333} + 2F_{1122} - 2F_{1133} - 2F_{2233} \\ +4F_{1212} - 4F_{1313} - 4F_{2323}) \\ F_{2222} + F_{3333} - 2F_{2233} - 4F_{2323} \\ 4F_{1112} - 4F_{3312} - 8F_{1223} - 8F_{1323} \\ 4F_{1113} - 4F_{3313} \\ 4F_{1123} - 4F_{3323} + 8F_{1213} \\ 4F_{2212} - 4F_{3312} - 8F_{1223} - 8F_{1323} \\ -4F_{3313} + 4F_{2213} \\ 4F_{2223} - 4F_{3323} \end{bmatrix}, \quad \text{(D53)}$$

$$\mathbf{V}^h = \begin{bmatrix} 0 \\ 1 \\ 0 \\ 0 \\ 0 \\ 0 \\ 0 \\ F_{11} - F_{33} \\ 2F_{12} \\ 2F_{13} \\ F_{22} - F_{33} \\ 2F_{23} \\ 0 \\ 0 \\ 0 \\ 0 \\ 0 \\ 0 \\ 0 \\ 0 \\ 0 \end{bmatrix}. \quad \text{(D54)}$$

Then from (14)-(16) and (B13)-(B19) we obtain

$$a = \frac{1}{4\pi} \int_{\theta=0}^{\pi} \int_{\varphi=0}^{2\pi} \eta_0(\theta, \varphi) sin(\theta) d\theta d\varphi$$

$$- \left(\frac{1}{4\pi} \int_{\theta=0}^{\pi} \int_{\varphi=0}^{2\pi} \eta_0 \mathbf{V}^d(\theta, \varphi) sin(\theta) d\theta d\varphi \right) \cdot \boldsymbol{\alpha} \cdot \boldsymbol{\alpha}$$

$$= a^0 - \mathbf{a}^d \cdot \boldsymbol{\alpha} \quad \text{(D55)}$$

$$b = \frac{1}{4\pi} \int_{\theta=0}^{\pi} \int_{\varphi=0}^{2\pi} \kappa_0(\theta, \varphi) sin(\theta) d\theta d\varphi$$

$$- \left(\frac{1}{4\pi} \int_{\theta=0}^{\pi} \int_{\varphi=0}^{2\pi} \kappa_0 \mathbf{V}^h(\theta, \varphi) sin(\theta) d\theta d\varphi \right) \cdot \boldsymbol{\alpha}$$

$$= b^0 - \mathbf{b}^d \cdot \boldsymbol{\alpha} \quad \text{(D56)}$$

$$U_{pq} = \frac{15}{8\pi} \int_{\theta=0}^{\pi} \int_{\varphi=0}^{2\pi} F_{pq}(\theta, \varphi) \eta_0(\theta, \varphi) sin(\theta) d\theta d\varphi$$

$$-\left(\frac{15}{8\pi}\int_{\theta=0}^{\pi}\int_{\varphi=0}^{2\pi}F_{pq}(\theta,\varphi)\eta_0\mathbf{V}^d(\theta,\varphi)sin(\theta)d\theta d\varphi\right)\cdot\boldsymbol{\alpha}$$
$$=U^0_{pq}-\mathbf{U}^d_{pq}\cdot\boldsymbol{\alpha} \tag{D57}$$

$$V_{pq}=\frac{15}{8\pi}\int_{\theta=0}^{\pi}\int_{\varphi=0}^{2\pi}F_{pq}(\theta,\varphi)\kappa_0(\theta,\varphi)sin(\theta)d\theta d\varphi$$
$$-\left(\frac{15}{8\pi}\int_{\theta=0}^{\pi}\int_{\varphi=0}^{2\pi}F_{pq}(\theta,\varphi)\kappa_0\mathbf{V}^h(\theta,\varphi)sin(\theta)d\theta d\varphi\right)\cdot\boldsymbol{\alpha}$$
$$=V^0_{pq}-\mathbf{V}^d_{pq}\cdot\boldsymbol{\alpha} \tag{D58}$$

$$Z_{pqrs}=\frac{315}{32\pi}\int_{\theta=0}^{\pi}\int_{\varphi=0}^{2\pi}F_{pqrs}(\theta,\varphi)\eta_0(\theta,\varphi)sin(\theta)d\theta d\varphi$$
$$-\left(\frac{315}{32\pi}\int_{\theta=0}^{\pi}\int_{\varphi=0}^{2\pi}F_{pqrs}(\theta,\varphi)\eta_0\mathbf{V}^d(\theta,\varphi)sin(\theta)d\theta d\varphi\right)\cdot\boldsymbol{\alpha}$$
$$=V^0_{pqrs}-\mathbf{V}^d_{pqrs}\cdot\boldsymbol{\alpha} \tag{D59}$$

Similarly as in the 2D case, the tensor can be written in the form

$$[\overline{\mathbf{C}}(\boldsymbol{\alpha})]=[\overline{\mathbf{C}}^0]-\tilde{\mathbf{C}}\cdot\boldsymbol{\alpha} \tag{D60}$$

where $[\overline{\mathbf{C}}(\boldsymbol{\alpha})]$ is a vector containing the components of $\overline{\mathbb{C}}(\boldsymbol{\alpha})$ as

$$[\overline{\mathbf{C}}(\boldsymbol{\alpha})]^T=\big[\,\overline{C}_{1111}(\boldsymbol{\alpha});\ \overline{C}_{1122}(\boldsymbol{\alpha});\ \overline{C}_{1133}(\boldsymbol{\alpha});\ ...$$
$$\overline{C}_{1212}(\boldsymbol{\alpha});\ \overline{C}_{1223}(\boldsymbol{\alpha});\ \overline{C}_{2323}(\boldsymbol{\alpha}),\big] \tag{D61}$$

and $\tilde{\mathbf{C}}$ is a matrix with the vectors $\mathbf{C}_{ijkl}$ as columns as

$$\tilde{\mathbf{C}}=\big[\,\mathbf{C}^T_{1111}\ \mathbf{C}^T_{1122}\ \mathbf{C}^T_{1133}...\ \mathbf{C}^T_{1212}\ \mathbf{C}^T_{1223}\ \mathbf{C}^T_{2323}\,\big] \tag{D62}$$

where the different vectors $\mathbf{C}_{ijkl}$ are obtained from (B20) and Eqs. (C36)-(C44) as:

$$\mathbf{C}_{1111}=\boldsymbol{\gamma}+2\boldsymbol{\beta}+2\mathbf{A}_{11}+4\mathbf{B}_{11}+\mathbf{Z}_{1111} \tag{D63}$$
$$\mathbf{C}_{1122}=\boldsymbol{\gamma}+\mathbf{A}_{11}+\mathbf{A}_{22}+\mathbf{Z}_{1122} \tag{D64}$$
$$\mathbf{C}_{1133}=\boldsymbol{\gamma}-\mathbf{A}_{22}-\mathbf{Z}_{1111}-\mathbf{Z}_{1112} \tag{D65}$$
$$\mathbf{C}_{1112}=\mathbf{A}_{12}+2\mathbf{B}_{12}+\mathbf{Z}_{1112} \tag{D66}$$
$$\mathbf{C}_{1113}=\mathbf{A}_{13}+2\mathbf{B}_{13}+\mathbf{Z}_{1113} \tag{D67}$$
$$\mathbf{C}_{1123}=\mathbf{A}_{23}+\mathbf{Z}_{1123} \tag{D68}$$
$$\mathbf{C}_{2222}=\boldsymbol{\gamma}+2\boldsymbol{\beta}+2\mathbf{A}_{22}+4\mathbf{B}_{22}+\mathbf{Z}_{2222} \tag{D69}$$
$$\mathbf{C}_{2233}=\boldsymbol{\gamma}-\mathbf{A}_{11}-\mathbf{Z}_{1122}-\mathbf{Z}_{2222} \tag{D70}$$
$$\mathbf{C}_{2212}=\mathbf{A}_{12}+2\mathbf{B}_{12}+\mathbf{Z}_{2212} \tag{D71}$$
$$\mathbf{C}_{2213}=\mathbf{A}_{13}+\mathbf{Z}_{2213} \tag{D72}$$
$$\mathbf{C}_{2223}=\mathbf{A}_{23}+2\mathbf{B}_{23}+\mathbf{Z}_{2223} \tag{D73}$$
$$\mathbf{C}_{3333}=\boldsymbol{\gamma}+2\boldsymbol{\beta}-2\left(\mathbf{A}_{11}+\mathbf{A}_{22}\right)$$
$$-4\left(\mathbf{B}_{11}+\mathbf{B}_{22}\right)+\mathbf{Z}_{1111}+\mathbf{Z}_{2222}+2\mathbf{Z}_{1122} \tag{D74}$$
$$\mathbf{C}_{3312}=\mathbf{A}_{12}-\mathbf{Z}_{1112}-\mathbf{Z}_{2212} \tag{D75}$$

$$\mathbf{C}_{3313} = \mathbf{A}_{13} + 2\mathbf{B}_{13} - \mathbf{Z}_{1113} - \mathbf{Z}_{2213} \quad \text{(D76)}$$

$$\mathbf{C}_{3323} = \mathbf{A}_{23} + \mathbf{B}_{23} - \mathbf{Z}_{1123} - \mathbf{Z}_{2223} \quad \text{(D77)}$$

$$\mathbf{C}_{1212} = \boldsymbol{\beta} + (\mathbf{B}_{11} + \mathbf{B}_{22}) + \mathbf{Z}_{1122} \quad \text{(D78)}$$

$$\mathbf{C}_{1213} = \mathbf{B}_{23} + \mathbf{Z}_{1123} \quad \text{(D79)}$$

$$\mathbf{C}_{1223} = \mathbf{B}_{13} + \mathbf{Z}_{2213} \quad \text{(D80)}$$

$$\mathbf{C}_{1313} = \boldsymbol{\beta} + (\mathbf{B}_{11} + \mathbf{B}_{22}) - \mathbf{Z}_{1111} - \mathbf{Z}_{1122} \quad \text{(D81)}$$

$$\mathbf{C}_{1323} = \mathbf{B}_{12} - \mathbf{Z}_{1112} - \mathbf{Z}_{2212} \quad \text{(D82)}$$

$$\mathbf{C}_{2323} = \boldsymbol{\beta} - \mathbf{B}_{11} - \mathbf{Z}_{1122} - \mathbf{Z}_{2222} \quad \text{(D83)}$$

and

$$\boldsymbol{\gamma} = \frac{1}{2}(\mathbf{b} - \mathbf{a}), \boldsymbol{\beta} = \frac{1}{4}(3\mathbf{a} - \mathbf{b}) \quad \text{(D84)}$$

$$\mathbf{a} = \mathbf{V} - \mathbf{U}, \quad \mathbf{B} = \frac{1}{4}(3\mathbf{U} - 2\mathbf{V}). \quad \text{(D85)}$$

References

[1] I.M. Gitman, H. Askes, and L.J. Sluys. Representative volume: Existence and size determination. *Engineering Fracture Mechanics*, 74(16):2518 – 2534, 2007.

[2] C. Pelissou, J. Baccou, Y. Monerie, and F. Perales. Determination of the size of the representative volume element for random quasi-brittle composites. *International Journal of Solids and Structures*, 46(14-15):2842 – 2855, 2009.

[3] R. Rezakhani, X. Zhou, and G. Cusatis. Adaptive multiscale homogenization of the lattice discrete particle model for the analysis of damage and fracture in concrete. *International Journal of Solids and Structures*, 125:50–67, 2017.

[4] G.A. Francfort and J.J. Marigo. Revisiting brittle fracture as an energy minimization problem. *Journal of the Mechanics and Physics of Solids*, 46(8):1319–1342, 1998.

[5] B. Bourdin, G.A. Francfort, and J.J. Marigo. Numerical experiments in revisited brittle fracture. *Journal of the Mechanics ad Physics of Solids*, 48:797–826, 2000.

[6] H. Amor, J.-J. Marigo, and C. Maurini. Regularized formulation of the variational brittle fracture with unilateral contact: Numerical experiments. *Journal of the Mechanics and Physics of Solids*, 57(8):1209–1229, 2009.

[7] C. Miehe, M. Hofacker, and F. Welschinger. A phase field model for rate-independent crack propagation: Robust algorithmic implementation based on operator splits. *Computer Methods in Applied Mechanics and Engineering*, 199:2776–2778, 2010.

[8] M. Ambati, T. Gerasimov, and L. de Lorenzis. A review on phase-field models of brittle fracture and a new fast hybrid formulation. *Computational Mechanics*, 55(2):383–405, 2015.

[9] J.-Y. Wu, V.P. Nguyen, C.T. Nguyen, D. Sutula, S. Bordas, and S. Sinaie. Phase field modeling of fracture. *Advances in Applied Mechanics: Multi-scale Theory and Computation*, 52, 2018.

[10] P.J. Rabier. Some remarks on damage theory. *International Journal of Engineering Science*, 27(1):29–54, 1989.

[11] J. Lemaitre. *A course on damage mechanics*. Springer Science & Business Media, 2012.

[12] W.C. Zhu and C.A. Tang. Micromechanical model for simulating the fracture process of rock. *Rock Mechanics and Rock Engineering*,

37(1):25–56, 2004.

[13] J.-Y. Wu and J. Li. On the mathematical and thermodynamical descriptions of strain equivalence based anisotropic damage model. *Mechanics of Materials*, 40(4-5):377–400, 2008.

[14] L. Olsen-Kettle. Bridging the macro to mesoscale: Evaluating the fourth-order anisotropic damage tensor parameters from ultrasonic measurements of an isotropic solid under triaxial stress loading. *International Journal of Damage Mechanics*, 28(2):219–232, 2019.

[15] J.L. Chaboche. Le concept de contrainte effective appliqué à l'élasticité et à la viscoplasticité en présence d'un endommagement anisotrope. In *Mechanical Behavior of Anisotropic Solids/Comportment Méchanique des Solides Anisotropes*, pages 737–760. Springer, 1982.

[16] M. Ortiz. A constitutive theory for the inelastic behavior of concrete. *Mechanics of Materials*, 4(1):67–93, 1985.

[17] J.C. Simo and J.W. Ju. Strain-and stress-based continuum damage models: I. formulation. *International Journal of Solids and Structures*, 23(7):821–840, 1987.

[18] S. Yazdani and H.L. Schreyer. Combined plasticity and damage mechanics model for plain concrete. *Journal of Engineering Mechanics*, 116(7):1435–1450, 1990.

[19] J. Lemaitre and J-L. Chaboche. *Mechanics of solid materials*. Cambridge University Press, 1994.

[20] V.A. Lubarda and D. Krajcinovic. Damage tensors and the crack density distribution. *International Journal of Solids and Structures*, 30(20):2859–2877, 1993.

[21] S. Govindjee, G.J. Kay, and J.C. Simo. Anisotropic modelling and numerical simulation of brittle damage in concrete. *International Journal for Numerical Methods in Engineering*, 38(21):3611–3633, 1995.

[22] G. Meschke, R. Lackner, and A.H. Man. An anisotropic elastoplastic-damage model for plain concrete. *International Journal for Numerical Methods in Engineering*, 42(4):703–727, 1998.

[23] J-L. Chaboche. Continuum damage mechanics: PartI and II. *Journal of Applied Mechanics*, 55(1):59–72, 1988.

[24] A. Cauvin and R.B. Testa. Damage mechanics: basic variables in continuum theories. *International Journal of Solids and Structures*, 36(5):747–761, 1999.

[25] P. Ladevèze. Sur une théorie de l'endommagement anisotrope. *Rapport interne No. 34, Laboratoire de Mécanique et Technologie*, 1983.

[26] Q.-C. He and A. Curnier. A more fundamental approach to damaged elastic stress-strain relations. *International Journal of Solids and Structures*, 32(10):1433–1457, 1995.

[27] Q.-C. He and A. Curnier. Characterising a 2D elasticity tensor by two orientation distribution functions. In *Proc. of 1994 IUTAM Symposium on "Anisotropy, Inhomogeneity and Nonlinearity in Solid Mechanics"*, pages 25–30, 1995.

[28] P. Ladevèze, D. Néron, and P.-W. Gerbaud. Data-driven computation for history-dependent materials. *Comptes Rendus Mécanique*, 347(11):831–844, 2019.

[29] F Ghavamian and A Simone. Accelerating multiscale finite element simulations of history-dependent materials using a recurrent neural network. *Computer Methods in Applied Mechanics and Engineering*, 357:112594, 2019.

[30] L. Wu, N.G. Kilingar, L. Noels, et al. A recurrent neural network-accelerated multiscale model for elasto-plastic heterogeneous materials subjected to random cyclic and non-proportional loading paths. *Computer Methods in Applied Mechanics and Engineering*, 369:113234, 2020.

[31] L. Wu, L. Adam, and L. Noels. Micromechanics and data-driven based reduced order models for multi-scale analyses of woven composites. *Composite Structures*, 270:114058, 2021.

[32] H. J. Logarzo, G. Capuano, and J.J. Rimoli. Smart constitutive laws: Inelastic homogenization through machine learning. *Computer Methods in Applied Mechanics and Engineering*, 373:113482, 2021.

[33] J.F. Unger C. and Könke. Coupling of scales in a multiscale simulation using neural networks. *Computers & Structures*, 86(21-22):1994–2003, 2008.

[34] G.A. Drosopoulos and G.E. Stavroulakis. Data-driven computational homogenization using neural networks: Fe2-nn application on damaged masonry. *Journal on Computing and Cultural Heritage (JOCCH)*, 14(1):1–19, 2020.

[35] C. He, J. Gao, H. Li, J. Ge, Y. Chen, J. Liu, and D. Fang. A data-driven self-consistent clustering analysis for the progressive damage behavior of 3d braided composites. *Composite Structures*, 249:112471, 2020.

[36] M.A. Benaimeche, J. Yvonnet, B. Bary, and Q.-C. He. A k-means clustering machine learning-based multiscale method for anelastic heterogeneous structures with internal variables. *International Journal for Numerical Methods in Engineering*, 123(9):2012–2041, 2022.

[37] J. Yvonnet, Q.-C. He, and P. Li. A data-driven harmonic approach to constructing anisotropic damage models with a minimum number of internal variables. *Journal of the Mechanics and Physics of Solids*, 162:104828, 2022.

[38] J.-C. Michel, H. Moulinec, and P. Suquet. Effective properties of composite materials with periodic microstructure: a computational approach. *Computer Methods in Applied Mechanics and Engineering*, 172:109–143, 1999.

[39] T.I. Zohdi and P. Wriggers. *An introduction to computational micromechanics*. Springer Science & Business Media, 2008.

[40] J. Yvonnet. *Computational Homogenization of Heterogeneous Materials with Finite Elements*. Springer Nature, 2019.

[41] P. Ladevèze. On an anisotropie damage theory. In *In: Failure Criteria of Structured media, J.P. Boehler (Ed.)*, pages 355–363, Balkema, Rotterdam, 1993.

[42] G. Backus. A geometrical picture of anisotropic elastic tensors. *Reviews of Geophysics*, 8(3):633–671, 1970.

[43] A.J.M. Spencer. A note on the decomposition of tensors into traceless symmetric tensors. *International Journal of Engineering Science*, 8(6):475–481, 1970.

[44] N. Moës, J. Dolbow, and T. Belytschko. A finite element method for crack growth without remeshing. *International Journal for Numerical Methods in Engineering*, 46(1):131–156, 1999.

[45] Z. Bažant and G. Pijaudier-Cabot. Nonlocal continuum damage, localization instability and convergence. *Journal of Applied Mechanics*, 55:521–539, 1988.

[46] F. Zhou and J.F. Molinari. Dynamic crack propagation with cohesive elements: a methodology to address mesh dependency. *International Journal for Numerical Methods in Engineering*, 59:1–24, 2004.

[47] N. Vilenkin. *Fonctions spéciales et théories de la représentation des groupes*. Dunod, 2010.

[48] M.N. Jones and M.N. Jones. *Spherical harmonics and tensors for classical field theory*, volume 2. Research Studies Press, 1985.

[49] E.T. Onat and F.A. Leckie. Representation of mechanical behavior in the presence of changing internal structure. *Journal of Applied Mechanics*, 55:1–10, 1988.

[50] J.L. Lumley. The structure of inhomogeneous turbulent flows. In *in: A.M. Yaglom, V.I. Tataski (Eds.), Atmospheric Turbulence and Radio Wave Propagation*, pages 166–178. Nauka, Moscow, 1967.

[51] K. Karhunen. Zur spektraltheorie stochastischer prozesse. *Ann. Acad. Sci. Fennicae*, 37, 1946.

[52] M.M. Loève. *Probability Theory*. Van Nostrand, NJ, 1955.

[53] H. Hotelling. Analysis of complex statistical variables in principal components. *Journal of Educational Psychology*, 24(6):417–444, 1953.

[54] C. Miehe, L.-M. Schaenzel, and H. Ulmer. Phase field modeling of fracture in multi-physics problems. part i. balance of crack surface and failure criteria for brittle crack propagation in thermo-elastic solids. *Computer Methods in Applied Mechanics and Engineering*, 294:449–485, 2015.